DETERMINATION OF MATRIX AND FRACTURE PERMEABILITIES IN WHOLE CORES USING PRESSURE PULSE DECAY

BY

KHALED SAEED BAJAALAH

A Thesis Presented to the

DEANSHIP OF GRADUATE STUDIES

KING FAHD UNIVERSITY OF PETROLEUM & MINERALS

DHAHRAN, SAUDI ARABIA

In Partial Fulfillment of the
Requirements for the Degree of

MASTER OF SCIENCE

In

PETROLEUM ENGINEERING

JUNE, 2009

KING FAHD UNIVERSITY OF PETROLEUM & MINERALS
DHAHRAN 31261, SAUDI ARABIA

DEANSHIP OF GRADUATE STUDIES

This thesis, written by **KHALED SAEED BAJAALAH** under the direction of his thesis advisor and approved by his thesis committee, has been presented to and accepted by the Dean of Graduate Studies, in partial fulfillment of the requirements for the degree of **MASTER OF SCIENCE IN PETROLEUM ENGINEERING**.

Thesis Committee

Dr. Hasan Y. Al-Yousef
Thesis Advisor

Dr. Hasan S. Al-Hashim
Member

Dr. Abdul-Aziz A. Al-Majed
Member

Dr. Sidqi A. Abu-Khamsin
Department Chairman

17/11/09

Dr. Salam Zummo
Dean of Graduate Studies (A)

عمادة الدراسات العليا
DEANSHIP OF GRADUATE STUDIES

DEDICATED

TO

MY PARENTS AND FAMILY

ACKNOWLEDGMENT

First and foremost thanks to Allah who gave me strength, patience and ability to accomplish this research.

Acknowledgment is due to the King Fahd University of Petroleum & Minerals for supporting this research.

I wish to express my appreciation to Dr. Hasan Y. Al-Yousef, who served as my major advisor, for his guidance and patience through the thesis, his continuous support and encouragement can never be forgotten. I would like also to thank my thesis committee member Dr. Hasan S. Al-Hashim and Dr. Abdul-Aziz A. Al-Majed for their suggestions and valuable comments. Thanks are also due to the Chairman of Petroleum Department Dr. Sidqi A. Abu-Khamsin for providing all the available facilities. I am also grateful to all faculty members for their encouragement and their direct or indirect help. Many thanks are also due to all the laboratory staff members in Petroleum and Gas Engineering Section, Research Institute for their cooperation and help during the experiment work.

Lastly, special thanks are due to my family members for their encouragement throughout my academic career. I also thank my friends in and out of campus who shared my happiness.

TABLE OF CONTENTS

LIST OF TABLES

LIST OF FIGURES

THESIS ABSTRACT

Name: **KHALED SAEED BAJAALAH**

Title: **Determination of Matrix and Fracture Permeabilities in Whole Cores Using Pressure Pulse Decay**

Major Field: **Petroleum Engineering**

Date of Degree: **June, 2009**

In recent years the pressure pulse decay technique became a frequent tool for fast and convenient measurement of permeability of tight rocks. The method is superior to conventional steady state method as it is much faster and easier to perform. Few authors considered measurement of matrix and fracture permeabilities by using this technique.

In this study a mathematical model for solving the problem of transverse, unsteady compressible fluid flow through fractured whole core was developed. Experimental setup has been constructed to perform pressure pulse decay experiments on whole cores. Based on the developed numerical solution, a data analysis computer program has also been developed which calculates the matrix and fracture permeabilities from pressure pulse decay experimental data using non-linear regression. A technique has also been presented for the estimation of the matrix and fracture permeabilities from pressure pulse decay tests.

MASTER OF SCIENCE DEGREE

KING FAHD UNIVERSITY OF PETROLEUM AND MINERALS
DHAHRAN, SAUDI ARABIA

JUNE 2009

ملخص الرسالة

الاســـــــــــم: **خالد سعيد احمد باجعاله**

عنوان الرسالة: **حساب نفادية الصخور الكاملة القطر المحتوية على صدع باستخدام طريقة تلاشي النبض الضغطي**

التخصـــــص: **هندسة بترول**

تاريخ التخـرج: **يونيو 2009 م**

لقد كثر استخدام طريقة تلاشي النبض الضغطي في حساب نفاذية الصخور المتماسكة جدا في الاونة الاخيرة وذلك لسهولة وسرعة اجراها مقارنة مع الطرق الاعتيادية. ولقد اجريت دراسات عديدة في تطوير هذه الطريقة واستخداماتها في حساب نفاذية الصخور المتماسكة جدا الا ان معظم هده الدرسات لم تتضمن استخدام هذه الطريقة في حساب نفاذية الصخور المحتوية على صدع.

وتهدف هذه الدراسة الى تطوير نموذج رياضي لحل مشكلة اعتراض السوائل غير منتظمة السريان والقابلة للانضغاط خلال سريانها عند العينات الصخرية الكاملة القطر المحتوية على صدع. بناءا على نتائج النموذج الرياضي فقد تم انشاء جهاز تقريبي لاداء تجارب التلاشي النبضي على العينات الصخرية الكاملة القطر المحتوية على صدع. ايضا فقد امكن تحليل النتائج باعداد برنامج حاسب الي يمكنه من حساب نفاذية الصخور المحتوية على صدع اعتمادا في الاساس على نتائج القياسات التجريبية للتلاشي النبضي باستخدام التراجع اللاخطي. ولقد قدم ايضا في هذه الدراسة اسلوب لتقدير نفاذية الصخور المحتوية على صدع من اختبارات تلاشي النبض الضغطي.

درجة الماجستير في العلوم

جامعة الملك فهد للبترول والمعادن

الظهران، المملكة العربية السعودية

يونيو 2009 م

CHAPTER 1

INTRODUCTION

The permeability of a reservoir rock is defined as the ability of fluids to pass through a porous material. The original work on permeability was carried out by H.Darcy (1856), who studied the flow rate of the springs at Dijon in France. His work was developed by Muskat and Botset. They formulated Darcy's law as follows

$$Q = \frac{k(P_1 - P_2)A}{\mu L} \tag{1-1}$$

Where

Q = Flow of rate

k = Permeability

$P_1 - P_2$ = Pressure drop across the sample

A = Cross sectional area of the sample

L = Length of the sample

μ = Viscosity of the fluid

Factors which influence effective porosity also influence permeability, namely, grain size, grain packing, grain angularity, grain size distribution, and degree of lithification. The permeability of a reservoir can be determined by three methods. On large scale it can be determined by means of drill stem or production test. The second method of determining permeability is by using correlations between permeability and wire line log responses. The third method of determining permeability is experimental by means of a permeameter using core samples.

Flow rate depends on the ratio of permeability to viscosity. Thus a gas reservoir may be able to flow with permeability of only a few md, whereas an oil reservoir needs minimal permeabilities of the order of tens md. For this reason low permeability is measured in the laboratory using gas rather than a liquid.

As many low permeability reservoirs worldwide still present a considerable potential for hydrocarbon production, determination of their permeability is usually difficult by the conventional steady state method because the flow rates are difficult to control and the measurement takes a long time. Brace et al.[6] introduced a transient technique, which is known as the pressure pulse decay for measuring permeability of tight rock with high accuracy and short time.

The presence of fractures in the reservoir changes the flow mechanism. In a fractured reservoir a network of fractures coexists with a network of matrix. The two porous networks have very different geometrical characteristics, porosities, capacities and permeabilities. Fracture permeability is much higher than matrix permeability and because of this; fluids flow mainly through the fracture. The ease with which fluids are exchanged between the matrix and the fracture depends on two factors:

- The geometry of matrix blocks.
- The ratio between matrix and fracture permeability.

Oil and gas production from naturally fractured reservoir is an important source of energy throughout the world. To better predict oil and gas flow rates petroleum engineers need to improve their understanding of naturally fractured reservoir. For this reason the measurement of matrix and fractures permeabilities are needed to be used in reservoir simulation models to predict the performance of naturally fractured reservoirs.

CHAPTER 2

BACKGROUND OF THE WORK

2.1 Literature review

2.1.1 Pressure pulse decay technique

Neilson [19] **(1966)** presented the idea of pressure pulse decay technique for measuring permeability of rocks. He did not introduce any mathematical details but only discussed the idea of pressure pulse decay technique, the experimental setup, and its advantages. He relied heavily upon the empirical interpretation methods based largely upon the time lapse between triggering and completion of the pressure decay.

Brace et al. [6] **(1968)** pioneered the pressure pulse decay technique for performing laboratory permeability measurements. They suggested a transient method, which was more convenient as the pressure and time are more easily measured in a high pressure experiment than flow rate. The mathematical model was based on the assumptions that the effect of rock compressibility is negligible compared with that of the pore fluid, and that the pore volume of the sample is negligible compared to the

volume of downstream vessel. They showed that the pressure gradient decays exponentially to zero. The pressure P_1 in the upstream reservoir was given as

$$(P_1 - P_f) = \Delta P\left[(V_2 / V_1) + V_2\right]e^{-\alpha t} \qquad (2\text{-}1)$$

Where

$$\alpha = (kA / \mu cL)(1/V_1 + 1/V_2) \qquad (2\text{-}2)$$

A = Cross sectional area

L = Length of the sample

V_1, V_2 = Volumes of upstream and downstream reservoirs

P_f = Final pressure

P_1 = Upstream reservoir pressure.

ΔP = Step change of pressure at t=0

μ = Viscosity of fluid

c = Compressibility of fluid

The permeability of a sample is found by plotting the pressure decay on semi log paper versus time. The slope of the resulting line is (-2.303α). The permeability is found from the equation 2.2.

Odeh and Mcmillen[22] **(1972)** introduced theoretical research for linear cores saturated with air on pulse propagation, and discussed how pulse tests in these systems can be analyzed to provide a measure of the permeability and porosity of porous medium. They also introduced an experimental work designed to compare these properties, as determined by conventional measurements, with those calculated from pulse test data. They noted that, when such pulse data are analyzed, the comparison has shown that the results are very favourable; i.e., differences in porosity values not more than 0.5 percent and differences in permeability values not more than 3 percent. They concluded that pulse experiments with linear cores saturated with air provide data, which when analyzed by methods based on the diffusion equation, give porosity and permeability values close to those obtained by conventional methods.

Yamada and Jones[31] **(1980)** introduced both mathematical formulation and numerical solution, which showed that the Brace et al.'s solution[6] can lead to error in calculating permeability if the pore volume of sample is not negligible compared with the upstream and downstream vessel volumes. They concluded that the pressure decay may look exponential, but it is only a fraction of an exponential curve, and the interpretation by Brace et al[6]. method cannot be applied.

Bourbie and Walls[5] **(1982)** proposed a new analytical solution known as error-function solution for the laboratory pulse decay permeability problem based on certain assumptions and specific boundary conditions. They also described Yamada and Jones'[29] numerical solution as inconvenient to use. They took the pore volume much smaller than the upstream and downstream reservoir volumes. The error resulting from using their exponential solution was about 25% and permeability calculated from their solution was within $\pm 5\%$ of steady state measurement over a wide range of permeability values.

Chen and Stagg[7] **(1984)** presented an alternative solution to the system of equations describing the pulse decay technique of permeability measurements. In this solution, pore volume was not neglected and the experimental data was analyzed by using the slope of a semi-log plot to determine permeability. This solution can also be used to analyze most core samples except those having extremely low permeability on the order of $10^{-6} md$. Here either the full solution given or the error-function solution must be used. They found that Brace et al.'s[6] solution underestimates the permeability and the degree of underestimation is dependent on the ratio of sample pore volume to downstream volume.

Amaefule et al.[2] **(1986)** discussed the application of transient pulse decay technique for determination of effective liquid permeabilities in low quality reservoir rock. Effective permeabilities of water and oil ranging from 0.5 to 290 $\times 10^{-4} md$ were determined by this technique. This technique developed for measurement of tight gas permeability, easily permits determination of effective permeability for oil and water with minimal pore volume throughput at low velocities.

They also reviewed mathematical computational techniques and outlined experimental procedures for accurate determination of liquid permeability in low quality rocks. They noted that the pulse decay technique is applicable for the measurement of effective permeability in whole cores and in fractured low permeability rocks. They concluded that the transient pulse decay technique is well suited for determination of effective permeability for oil and water in low quality rocks, and also using of the 'zero-porosity' approximation for permeability calculation by the transient technique can lead to substantial errors.

Haskett, Narahara and Holditch[14] **(1988)** introduced an analytical model for unsteady state gas flow through a core. This analytical model can be used in conjunction with a history matching technique to evaluate the porosity and permeability. There are only two unknowns, i.e., porosity and permeability in history matching. Because the

final pressure is solely dependent on porosity, a unique match of porosity for any given pressure decay is essentially ensured because the final pressure is solely dependent on porosity. The single best value for permeability is fixed because the porosity is also fixed. The results from this method showed good agreement with both actual core data and numerically simulated data.

Dicker and Smits[9] **(1988)** presented a new pressure pulse method to measure permeability of tight rock samples, which is simple and accurate and enable very fast permeability measurements when taking the volumes of the upstream and the downstream vessels in the equipment approximately equal to the pore volume of the sample. They also assumed that gas slippage effect is negligible because high pore pressure is used. The permeability can be calculated from the following equation:

$$k = \frac{c\mu\phi L^2 s}{f(a,b)} \tag{2-3}$$

Where

k = sample permeability

c = fluid compressibility

μ = fluid viscosity

ϕ = sample porosity

L = sample length

s = semi-log slope of the pressure decay ($\sec^{-1}$).

$$f(a,b) = (a+b+ab) - (a+b+0.4132ab)^2/3 + 0.0744(a+b+0.0578ab)^3$$

$$a = V_s/V_1 \quad \text{and} \quad b = V_s/V_2$$

V_s = sample pore volume, V_1 & V_2 = upstream and downstream reservoir volumes.

The method consists of plotting the measured pressure difference versus time on semi-log paper, determining the slope of the straight line part of this plot and calculating (k) from the above equation. They also suggested taking the volume of the upstream and the downstream vessels slightly smaller than the pore volume, such a and b are relatively large, resulting in fast measurements, whereas the simple analytical approximation is still valid.

Gilicz[10] **(1991)** applied the pulse decay technique for radial cores. He also presented the experimental set up, analytical solution of the governing equations and their application to the measurements. His analytical solution is general; no assumptions of negligible pore volume storage were made. The core pressure response is to be matched with analytical solution to determine porosity and permeability. The results

obtained by this method were in agreement with conventionally obtained porosity and permeability values.

Kamath, Boyer and Nakagawa[17] **(1992)** developed a new analytical method and an experimental set up to accurately and rapidly measure the permeability of homogeneous cores, matrix and fracture properties of fractured rocks and the individual properties of a butted core sample. Some of their important conclusions are:

- The effective permeability calculated from a transient test could be a function of the direction of the pressure disturbance and could differ significantly from the effective steady state value for heterogeneous cores.

- The pressure transient response of heterogeneous core appears similar to that of a homogeneous core for small ratio of the compressive storage of core to upstream vessel. Therefore, their pressure transient testing system contains variable volume vessels.

Guo and Wong[11] **(1996)** introduced an alternative method to perform pressure pulse decay tests without using upstream and downstream vessels. Mobility is calculated from pressure pulse decay in the sample using the finite difference method. Advantages of this method include high speed, ability to analyze poorly controlled upstream and

downstream pressure and the elimination of reservoirs. The estimated values from this method are comparable to those obtained from steady state measurements.

Jones[15] **(1997)** recommended that laboratory pulse decay measurements using a gas or liquid are effective for determining the permeability of rocks in the range from 0.1 *md* to 0.01 μd. This can be extended to 1 *md* or higher by using lager fluid reservoir. The actual measurement time with this pressure transient technique is fairly short, but pressure pre-equilibration sometimes requires hours. In this study he showed how the total time can be decreased significantly, especially if the pore volume of sample is measured independently or estimated accurately. He also recommended that permeability should be calculated from late time measurements for minimizing errors and increasing sample throughput.

He suggested that upstream and downstream reservoir volumes should be equal. This produces the desirable effects of maintaining a constant mean pore pressure during the single exponential portion of the decay and promotes its earlier onset. He noted that the time consuming initial pressure equilibration step can be eliminated using a modified technique in which a smooth pressure gradient is established from quasi steady state fluid flow from and to large reservoir. He also showed that the smaller reservoir volumes should be 2 to 10 times larger than the pore volume of the sample.

Hamid Jalal[12] **(2000)** extended the application of pressure pulse decay method from linear core plugs to full diameter whole cores and also developed a mathematical model. He calculated the permeability and klinkenberg factor from measured pressure pulse decay experimental data using non-linear regression technique. He noted that the pressure pulse decay method was much faster and easier to perform as compared to the conventional steady state method and could also help detect core heterogeneity. He concluded that the use of large pressure pulse in pulse decay experiments can introduce non-Darcy flow effect thus leading to underestimation of permeability and the selection of the optimum pulse size depends on the permeability of the sample and the size of the upstream and downstream cells.

Noman Muhammad[21] **(2000)** developed a computer model to analyze the pressure pulse decay data by taking into account the effects of gas slippage and non-Darcy flow. He noted that due to the opposite effects of gas slippage and non-Darcy flow on the pressure decay, it is not reliable to find the values of permeability, klinkenberg constant and forchherimer constant from a single pressure pulse decay test. Hence separate tests should be designed and performed to find klinkenberg constant and forchherimer constant with permeability.

2.1.2 Natural fractured reservoir

Warren and Root[30] **(1963)** developed an idealized model for studying the characteristic behaviour of a permeable medium. Their model is based on the following assumptions:

- The material contain the primary porosity is homogeneous and isotropic.
- Uniform fracture.
- Flow through the primary porosity elements cannot occur.

They noted that the following conclusions can be drawn as a result from their study:

- The storativity ratio, ω, and interporosity flow coefficient, λ, are the main parameters which are sufficient to characterize the deviation of the behaviour of a homogeneous porous media from that of a medium with double porosity.

- The proper analysis of pressure build up data gotten from designed test can be used to evaluate these parameters.

Odeh[23] **(1964)** developed a mathematical model to describe the unsteady state behaviour of naturally fractured reservoir. His model is based on the following assumptions:

- The matrix blocks act like sources.
- The net fluid movement toward the well bore gets only in the fractured.
- The flow capacity and degree of fracturing reservoir are uniform.

He noted that the following conclusions can be drawn as a result from his study:

- Fracture reservoir, described by this model, cannot be distinguished from homogeneous reservoirs on the basis of drawdown and build-up curves.
- It should be re-emphasized that all fractured reservoirs may not necessarily adapt to this analysis. The assumption of homogeneous fracturing may not apply to every fracture reservoir.

Kazem[18] **(1969)** developed an ideal theoretical model of a naturally fractured reservoir with a uniform fracture distribution. This model consists of a finite circular reservoir with a centrally located well and two distinct porous regions, referred to as matrix and fracture, respectively. The matrix has high storage, but low flow capacity; the fracture has low storage, but high flow capacity. The general assumptions of his model are:

- The flow is single phase
- The matrix flows into the fractures and then the fluid flows through the fractures to the wellbore.
- The flow is unsteady state
- The fracture and matrix are homogeneous and isotropic and the reservoir is horizontal.
- The well is centrally located in a finite circular reservoir.

He concluded that:

- The fractured reservoir characterizations of Warren-Root[30] are applicable to the cases where the fracture distribution is uniform and the contrast between fracture and matrix flow capacities is large. Thus, from a build-up test, the total flow capacity and ratio of storage capacities in such double porosity systems should be obtainable.

- Combining the results of an interference test and a build-up test on the same well should yield an approximate value for matrix permeability.

- Whenever the ratio of flow capacities in the matrix and in the fracture is small, only one straight line is noticeable, and this is in accordance with Odeh's conclusions [23].

- Pollard's [25] plot of pressure build-up seems to have only an apparent validity in evaluating fracture-matrix pore volumes.

- The behaviour of a fractured reservoir approaches that of an equivalent system of homogeneous reservoir at large times.

Asfari and Witherspoon [4] (1973) presented mathematical models by using the finite element method to understand the behaviour of naturally fractured reservoirs. They showed that the steady state solutions demonstrate how the effective permeability of the fractured system depends on both fracture conductivity and dimensionless parameters representing fracture density by changing permeability of the fracture relative to the matrix.

They concluded that they are able to investigate the variation of permeability anisotropy with the dimensionless parameters *l/d* and *l/s* by choosing a representative elemental area that is associated with a single fracture. For regular systems of fractures,

the permeability anisotropy increases with *l/s* for any given value of *l/d* and approaches an asymptotic value defined by 1 + *l/d*. This is true over the range of $10^3 < \frac{k_f}{k_m} < \infty$. They also noted that excellent agreement was obtained between these results and those developed by Prats[22], who used an analytic expression to relate permeability anisotropy to the fracture geometry of infinitely conductive fractures.

Ning, Fan, Holdtch and lee[20] (1993) described a new laboratory technique to evaluate the properties of naturally fractured low permeability core samples. They specifically determine:

1. The porosity of the matrix.
2. The permeability of the matrix.
3. The effective width of the fractures.
4. The permeability of the fractures.

Matrix permeability as low 10^{-9} *md* can be measured with this technique. A set of new analytical solutions describing gas flow in a fractured core during a pressure pulse test has been developed. The analytical solutions agree with finite difference simulation. They designed a laboratory equipment to perform pressure pulse measurement in either a fractured core sample or a homogeneous core sample.

Alan[1] **(1995)** described fractured reservoirs using a combination of high resolution geometrical information from borehole images together with deeper penetrating log evaluation methods. He noted that borehole images from acoustic or electrical scanning tools provide statistics of fracture distribution, first order estimates of fracture opening and porosity, and a basis for geological inference. In his study, he assumed that in basement rocks the pore shape controls the compressional and shear slownesses and that one or two typical pore aspect ratios can be derived by other means. He concluded that low-frequency acoustic waveform logs provide a robust means to evaluate fractures in basement reservoirs, and reducing the frequency reduces the sensitivity of the logs to borehole conditions and averages the formation properties. In addition to the well-known Stoneley wave techniques for deriving permeability and fracture aperture, the compressional and shear slownesses may be used to estimate both conventional and fracture porosity.

Sabathier, Bourbiaux, and Sarda[27] **(1998)** described the complete methodology and detail the specific fracture-matrix flow formulation, which could be input in other dual-porosity simulators. They presented cases which indicate that geologists and engineers can cooperate in a really- integrated fractured reservoir study based on a realistic picture of the fracture network. In addition, the modification of the matrix-fracture flow terms improves the model accuracy and speeds up the study as it does not require preparing any pseudo curve.

They concluded that their approach of fractured reservoirs is based on newly-developed methodologies, software tools and computation procedures which enable to integrate as much as possible of the information referring to the static image and the dynamic behaviour of the reservoir. They also noted that there are three major improvements contributed to the applicability of this approach to reservoir engineering:

- The possibility to generate representative geological images of the fractured medium from increasingly detailed and various field information about natural fracturing;

- The availability of software enabling to process these images in order to determine the equivalent hydraulic parameters required as input for the dual-porosity model to be used for multiphase flow simulations;

- The use of a general formulation of matrix-fracture transfers which can reliably account for the various physical mechanisms of flow exchanges at matrix block scale.

Baker and Kupper[26] **(2000)** evaluated three field studies combining the "forward" modelling approach, typically used by geoscientists, with "inverse" techniques, usually incorporated by reservoir engineers. The inverse approach focuses

more on the effect created by the naturally fractured reservoir (e.g. material balance, decline analysis, productivity, etc.) while the forward approach examines various causes of natural fractures and its' associated properties (e.g. fracture spacing, height, stress distribution, etc.). They also showed how a more powerful methodology is created, for the evaluation of naturally fractured reservoirs, when combining two techniques that have, historically, been applied in relative isolation. Some of their important conclusions are:

- Forward and Inverse methods do not characterize the fracture network sufficiently, when used in isolation, because fracture connectivity is unknown. Combining these two techniques provides a more powerful complementary means of doing so.

- Fracture heterogeneity is often over-simplified, or "smeared" in simulation models by using an insufficient number of layers or grid blocks. It is important to preserve the high permeability, high intensity fracture zones to accurately model breakthrough trends and ultimate recovery.

Sandro, Eduardo and Hector[28] **(2004)** introduced a new methodology to identify fractured intervals in a naturally fractured reservoir by combining the answer of a set of conventional electric logs and the information coming from the physical

description of the cores of a fractured formation. They noted that with this information, a continuous variable fracture intensity track is generated and related with the fracture permeability through two different approaches. In the first approach, the aperture and fracture intensity were used to estimate the fracture permeability. The second approach is indirect. Using a non-parametric regression technique, the measured fracture permeability is modelled from variables such as gamma ray, fracture porosity, Farcies, and fracture intensity. They successfully applied the proposed technique on a reservoir producing from a Cretaceous Formation in a Colombian Field. Some of their important conclusions are:

- They developed an analytic expression that demonstrates the dependence of the fracture permeability on the fracture intensity.

- A model was generated to determine the fracture permeability departing from indirect determinations (FACIE, GR. LOGFRAC and PHIE) and the use of the GRACE algorithm.

- It was demonstrated, in the wells of the area, the relative effect of the fracture intensity on the fracture permeability and productivity for a NFR.

2.2 Statement of the Problem

It is apparent from the preceding literature review that a lot of work has been done in the development and application of pressure pulse decay technique for measuring the matrix permeability of tight rocks. But only a few of the authors considered measurement of the fracture and matrix permeabilities by using pulse decay technique.

For the case of measuring permeability of the core sample, the most reliable and direct way to determine the formation properties is to obtain a core from the reservoir and to measure the permeability in the laboratory. However, conventional laboratory methods cannot be used to measure the properties of the fracture and matrix in a naturally fractured core. Existing laboratory methods can only measure the effective permeability of a core sample if the core sample contains fractures. Furthermore, the fracture and matrix properties cannot be distinguished by using existing laboratory techniques.

Thus, there is a need to investigate the application of the pressure pulse decay technique to measure the fracture and matrix permeabilities of whole cores.

2.3 Objectives and approach of the study

2.3.1 Objectives of the study

The main objectives of this study are the following:

- To develop a mathematical model and obtain solution to describe the pressure pulse behaviours in a fractured core sample.

- To construct a laboratory experimental setup with appropriate upstream and downstream volumes. Use the setup to conduct pressure pulse decay experiments and analyze the data to obtain fracture and matrix permeabilities.

- To validate the mathematical model results.

2.3.2 Approach of the study

In order to achieve the objectives of the study, the following proposed approach will be followed.

- Develop a mathematical model and obtain solution to describe pressure pulse decay in a fractured core.

- Use the solution to design the pressure pulse decay experiment and obtain appropriate experimental conditions.

- Construct a pressure pulse decay setup and calibrate it.

- Perform pressure pulse decay experiments.

- Analyze the data to obtain matrix and fracture permeabilities.

CHAPTER 3

MATHEMATICAL MODEL

The description of the mathematical model developed for this study is presented in this chapter. Furthermore, the finite difference representation of governing differential equation and grid system development are also presented in this chapter.

3.1 The model flow equation

The governing equation which was developed for the transient flow of compressible fluids in porous media was based on the following assumptions:

1. The flow is isothermal.
2. The flow is single phase.
3. Two dimensional flow.
4. Rock properties like permeability and porosity are constant.
5. Isotropic and heterogeneous porous media.

The basic equation which describes the transient flow of real gas in porous media was derived based on the principle of conservation of mass, kilinkenberg equation,

Darcy's law and the equation of state. In the radial coordinate system, the flow equation of the model is given as

For fracture:

$$\frac{1}{r}\frac{\partial}{\partial r}\left[r\frac{P_f}{\mu z}\left(1+\frac{b}{P_f}\right)\frac{\partial P_f}{\partial r}\right]+\frac{1}{r^2}\frac{\partial}{\partial \theta}\left[\frac{P_f}{\mu z}\left(1+\frac{b}{P_f}\right)\frac{\partial P_f}{\partial \theta}\right]-\frac{\lambda P_m}{\mu z}\left(P_f-P_m\right)=\frac{\varphi_f c_{tf}}{k_f}\frac{P_f}{z}\left(\frac{\partial P_f}{\partial t}\right) \tag{3-1}$$

For matrix:

$$\frac{1}{r}\frac{\partial}{\partial r}\left[r\frac{P_m}{\mu z}\left(1+\frac{b}{P_m}\right)\frac{\partial P_m}{\partial r}\right]+\frac{1}{r^2}\frac{\partial}{\partial \theta}\left[\frac{P_m}{\mu z}\left(1+\frac{b}{P_m}\right)\frac{\partial P_m}{\partial \theta}\right]+\frac{\lambda P_m}{\mu z}\left(P_f-P_m\right)=\frac{\varphi_m c_{tm}}{k_m}\frac{P_m}{z}\left(\frac{\partial P_m}{\partial t}\right) \tag{3-2}$$

Where

P_f = Pressure in fracture.

P_m = Pressure in matrix.

μ = Gas viscosity.

z = Gas deviation factor.

b = Gas slippage.

k_f = Permeability in fracture.

k_m = Permeability in matrix.

φ_f = Porosity in fracture.

φ_m = Porosity in matrix.

c_{tf} = Total compressibility in fracture.

c_{tm} = Total compressibility in matrix.

λ = Interporosity flow parameter.

h = Thickness

A typical pressure pulse decay experimental set-up for measuring permeability of whole core sample is shown in Figure 3.1. There are two mesh screens of equal width and covering a subtended angle (θ) which are placed on opposite ends of the core sample parallel to the axis of core. Also a rubber sleeve is fitted around the core and the screens to prevent any bypass flow around the core.

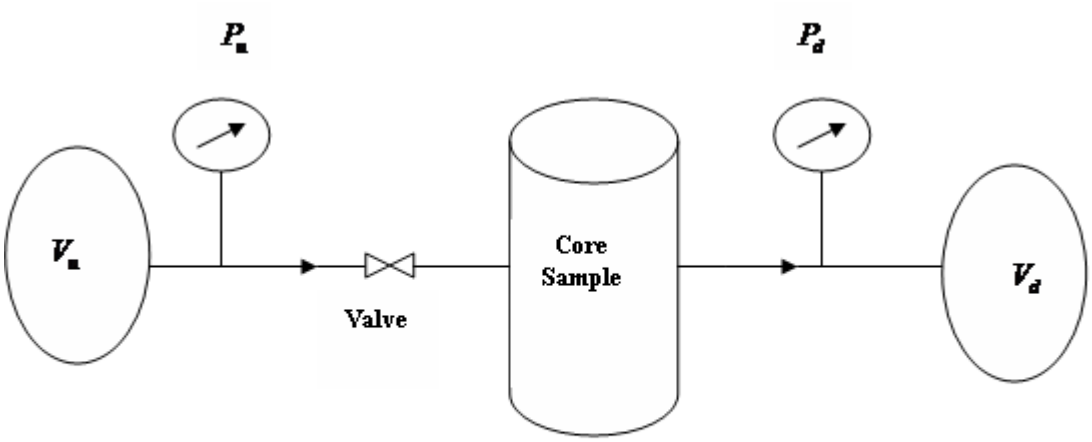

Figure 3-1 Schematic of pressure pulse decay for measuring permeability of whole cores

3.2 Initial and boundary conditions

3.2.1 Initial condition

At t = 0,

$$P_u(0) = P_u \qquad \text{For upstream vessel} \qquad (3\text{-}3)$$

$$P_d(0) = P_d \qquad \text{For downstream vessel and core sample} \qquad (3\text{-}4)$$

3.2.2 Boundary conditions

Figure 3.2 shows the boundary conditions, in this plot, only one half of circle is considered.

At t > 0,

$$P_m(r,\theta,t) = P_f(r,\theta,t) = P_u(t) \quad \text{For} \quad 0 \le \theta \le \theta_s \qquad (3\text{-}5)$$

$$P_m(r,\theta,t) = P_f(r,\theta,t) = P_d(t) \quad \text{For} \quad (\pi - \theta_s) \le \theta \le \pi \qquad (3\text{-}6)$$

$$c_g V_u \frac{\partial P_u}{\partial t} = \frac{1}{CF}\frac{k_m h}{\mu}\left(1 + \frac{b_m}{p_m}\right)\int_0^{\theta} r \frac{\partial P_m}{\partial r} d\theta + \frac{1}{CF}\frac{k_f h}{\mu}\left(1 + \frac{b_f}{p_f}\right)\int_0^{\theta} r \frac{\partial P_f}{\partial r} d\theta \Big|_{r=R_c}$$

For $0 \le \theta \le \theta_s$ (3-7)

$$c_g V_d \frac{\partial P_d}{\partial t} = \frac{1}{CF}\frac{k_m h}{\mu}\left(1+\frac{b_m}{p_m}\right)\int_{\pi-\theta_s}^{\pi} r\frac{\partial P_m}{\partial r}d\theta + \frac{1}{CF}\frac{k_f h}{\mu}\left(1+\frac{b_f}{p_f}\right)\int_{\pi-\theta_s}^{\pi} r\frac{\partial P_f}{\partial r}d\theta \quad {}^{r=R_c}$$

For $(\pi-\theta_s) \le \theta \le \pi$ (3-8)

Where

R_c = Radius of whole core sample.

P_u *and* P_d = Pressure in the upstream and downstream vessels.

V_u *and* V_d = Volume of the upstream and downstream vessels.

CF = Unit conversion factor.

c_g = Gas compressibility.

The remaining surface of the core sample is a no-flow boundary

$$\left.\frac{\partial P}{\partial r}\right|_{r=R_C} = 0 \qquad (3\text{-}9)$$

Equation (3.3) states that at the start of the experiment, the pressure at the inlet face is equal to the upstream vessel pressure while equation (3.4) states that the pressure

in the sample is equal to the downstream vessel pressure. Equations (3.5) and (3.6) indicate that the upstream and downstream faces of the sample are in direct contact with their respective vessel. Equations (3.7) and (3.8) express mass conservation at the sample face, for example, fluid flow from the sample results in a pressure increase in the downstream vessel.

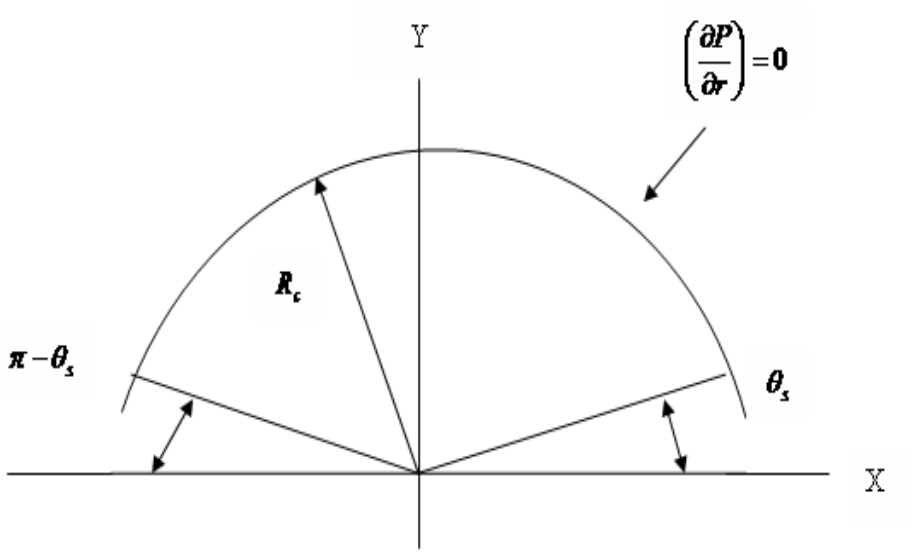

Figure 3-2 Boundary condition for the transverse flow

3.3 The numerical model

Many researchers have proposed to use the curvilinear coordinate system as a choice to Cartesian and radial coordinates for the simulation of complex flow geometries. Hirasaki and Odell[13] suggested that adopting curvilinear coordinate results in more accurate model for the flow geometry for complex permeability. They also presented the finite difference equations which were different from the standard formulation using Cartesian coordinates. They included transmissibilities caused by the metric tensor and a factor multiplying the pore volume. Sonier and Chaurnet[29] suggested to write the finite difference equations related to the mass conservation equations without going through metric tensors due to the latter would be too difficult to compute in general cases.

For our system, curvilinear coordinates that coincide with the orthogonal network of isopotential lines and stream lines of steady state single phase flow were developed. The solution of the Laplace equation for homogeneous and isotropic is based on the isopotential and stream lines obtained by using the conformal mapping technique. This includes combining the stream line $(\psi)$and a complex potential $(w(z))$ with potential(ϕ). When $(w(z))$is obtained, the stream line (ψ) is the imaginary part of $(w(z))$and (ϕ) is the real part of$(w(z))$.

Collins[8] introduced conformal transformation equations for transverse permeability problem given by:

$$w = -i \ln\left(\frac{z}{R}\right) \tag{3-10}$$

Where R is the radius of the core sample. This describes the region of flow as semi-infinite strip in the (w) plan and then, a second conformal mapping was:

$$w'_{\cdot} = \frac{\sin(w)}{K} \tag{3-11}$$

The above step describes the transforms region of flow into the whole upper half of the (w') plan. Where

$$K = \sin\left(\frac{\pi}{2} - \theta_s\right) = \cos(\theta_s) \tag{3-12}$$

Finally, taking the inverse of the transformation Equation (3.13) is obtained.

$$w' = \int_0^{w''} \frac{d\xi}{\left(1-\xi^2\right)^{1/2}\left(1-k^2\xi^2\right)^{1/2}} \tag{3-13}$$

Equation (3.13) states that the flow region is transformed into the rectangle in (w'')plane. All series of conformal mappings are plotted in Figure (3.3). Figure (3.4) shows the grid system after applying the same transformation in reverse order.

If the isopotential lines and the stream lines are used as coordinate system, then, the governing partial differential equation for our system is given as:

For fracture

$$\frac{\partial}{\partial\phi}\left[F\frac{\partial P_f}{\partial\phi}\right]+\frac{\partial}{\partial\psi}\left[F\frac{\partial P_f}{\partial\psi}\right]-\sqrt{g}H\lambda\left(P_f-P_m\right)=CF\sqrt{g}\,\frac{\varphi_f}{k_f}G\left(\frac{\partial P_f}{\partial t}\right) \tag{3-14}$$

For matrix:

$$\frac{\partial}{\partial\phi}\left[F\frac{\partial P_m}{\partial\phi}\right]+\frac{\partial}{\partial\psi}\left[F\frac{\partial P_m}{\partial\psi}\right]+\sqrt{g}H\lambda\left(P_f-P_m\right)=CF\sqrt{g}\,\frac{\varphi_m}{k_m}G\left(\frac{\partial P_m}{\partial t}\right) \tag{3-15}$$

Where

$$F=\frac{P+b}{\mu z}$$

$$G=\frac{Pc_t}{z}$$

$$H = \frac{P_m}{\mu z}$$

CF = Unit conversion factor

$\sqrt{g}$ = Determinant of the metric tensor

The matrix tensor relates increments of distance, area and volume to product of coordinate increments. It may be interpreted as "shape operator" which relates a curved grid block in a curvilinear coordinate system to a rectangular grid block in Cartesian coordinate system[12] .

Due to the non-linearity of equations (3.14) and (3.15), it is difficult to get an analytical solution for the transient compressible fluid flow equations. Thus a numerical solution has been developed to solve the governing partial differential equations.

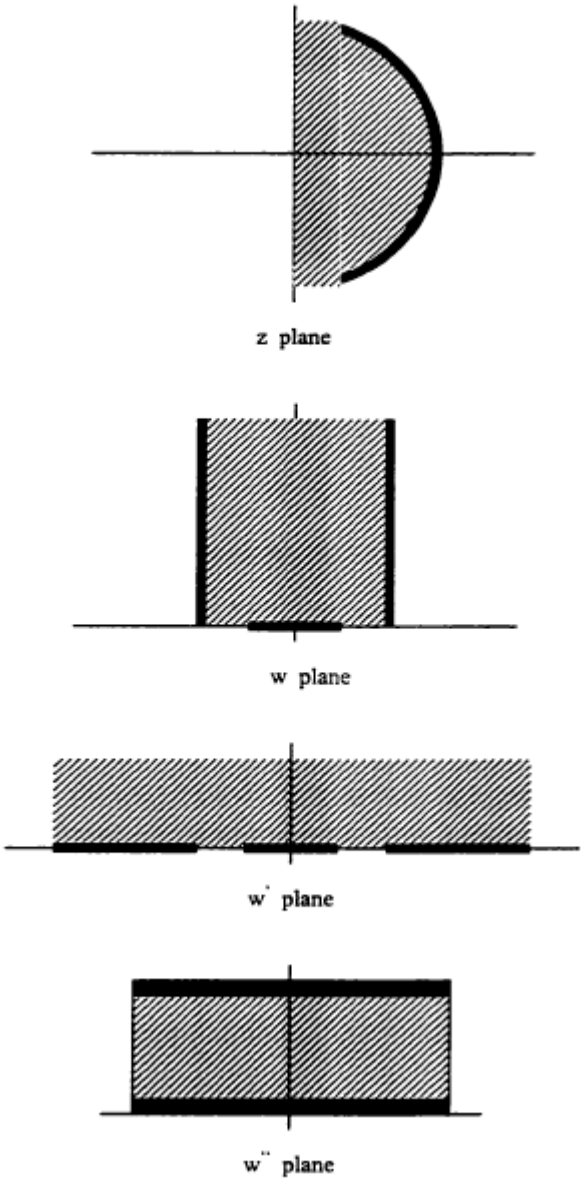

Figure 3-3 Conformal mapping of transverse permeability problem [8]

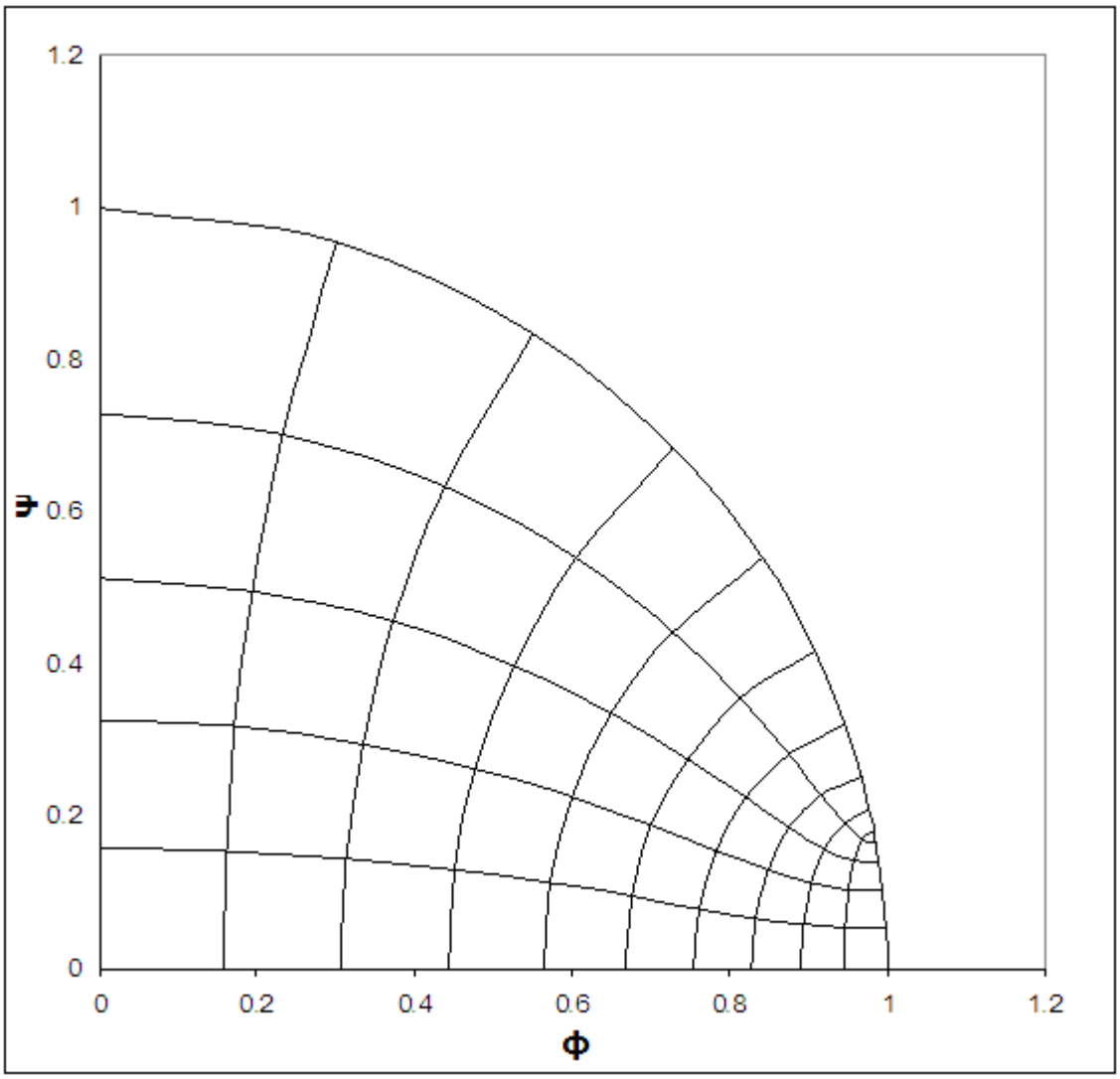

Figure 3-4 The curvilinear coordinates grid system

3.4 Finite difference equation

Finite difference technique was used to solve Equations (3.14) and (3.15) which describe the fluid flow in curvilinear coordinates system. To get the solution and determine the permeabilities of fracture and matrix from the measured experimental data for whole core samples, a single-phase two dimensional finite difference model was used while a single-phase one dimensional finite difference model was used for core flow along the length of the sample.

3.4.1 Finite difference equation for one dimensional

The Partial differential equation for one dimensional transient flow of gas through porous media is given as:

For fracture

$$\frac{\partial}{\partial x}\left[k_f A_f \frac{P_f}{\mu z}\left(1+\frac{b_f}{P_f}\right)\frac{\partial P_f}{\partial x}\right]-\lambda A\frac{P_m}{\mu z}\left(P_f-P_m\right)=\phi_f A_f c_t \frac{P_f}{z}\frac{\partial P_f}{\partial t} \tag{3-16}$$

For matrix

$$\frac{\partial}{\partial x}\left[k_m A_m \frac{P_m}{\mu z}\left(1+\frac{b_m}{P_m}\right)\frac{\partial P_m}{\partial x}\right]+\lambda A\frac{P_m}{\mu z}\left(P_f-P_m\right)=\phi_m A_m c_t \frac{P_m}{z}\frac{\partial P_m}{\partial t} \tag{3-17}$$

To get numerical or analytical solutions of equations 3-16 and 3-17 the initial and boundary conditions must be specify. These initial and boundary conditions are given below

$$P_m(0,t) = P_f(0,t) = P_u(t) \quad \text{for} \quad t \geq 0 \tag{3-18}$$

$$P_m(L,t) = P_f(L,t) = P_d(t) \quad \text{for} \quad t \geq 0 \tag{3-19}$$

$$c_g V_u \frac{\partial P_u}{\partial t} = \frac{1}{CF}\frac{k_f A_f}{\mu}\frac{(b_f + P_f)}{P_f}\frac{\partial P_f}{\partial x} + \frac{1}{CF}\frac{k_m A_m}{\mu}\frac{(b_m + P_m)}{P_m}\frac{\partial P_m}{\partial x} \quad \text{for } t > 0 \tag{3-20}$$

$$c_g V_d \frac{\partial P_d}{\partial t} = \frac{1}{CF}\frac{k_f A_f}{\mu}\frac{(b_f + P_f)}{P_f}\frac{\partial P_f}{\partial x} + \frac{1}{CF}\frac{k_m A_m}{\mu}\frac{(b_m + P_m)}{P_m}\frac{\partial P_m}{\partial x} \quad \text{for } t > 0 \tag{3-21}$$

After applying the boundary conditions, the finite difference equations are given as:

Cell i = 1 (Upstream cell):

$$\left[a_1 F_{mi+1/2} + a_2 F_{fi+1/2} + V_u G_i\right]P_i^{n+1} + \left[-a_1 F_{mi+1/2}\right]P_{mi+1}^{n+1} + \left[-a_2 F_{fi+1/2}\right]P_{fi+1}^{n+1} = V_u G_i P_i^n \tag{3-22}$$

Cell i = 2 to N-1(Core Sample):

i = 2

For fracture

$$\left[-2a_4F_{fi-1/2}\right]P_{fi-1}^{n+1}+\left[a_4F_{fi+1/2}+2a_4F_{fi-1/2}+\lambda\Delta xA\Delta tH+V_{pfi}G_{fi}\right]P_{fi}^{n+1}+\left[-a_4F_{fi+1/2}\right]P_{fi+1}^{n+1}$$
$$-\lambda\Delta xA\Delta tHP_{mi}^{n+1}=V_{pfi}G_{fi}P_{fi}^{n}$$

(3-23)

For matrix

$$\left[-2a_3F_{mi-1/2}\right]P_{mi-1}^{n+1}+\left[a_3F_{mi+1/2}+2a_3F_{mi-1/2}+\lambda\Delta xA\Delta tH+V_{pmi}G_{mi}\right]P_{mi}^{n+1}+\left[-a_3F_{mi+1/2}\right]P_{mi+1}^{n+1}$$
$$-\lambda\Delta xA\Delta tHP_{fi}^{n+1}=V_{pmi}G_{mi}P_{mi}^{n}$$

(3-24)

i = 3 to N-2

For fracture

$$\left[-a_4F_{fi-1/2}\right]P_{fi-1}^{n+1}+\left[a_4F_{fi+1/2}+a_4F_{fi-1/2}+\lambda\Delta xA\Delta tH+V_{pfi}G_{fi}\right]P_{fi}^{n+1}+\left[-a_4F_{fi+1/2}\right]P_{fi+1}^{n+1}$$
$$-\lambda\Delta xA\Delta tHP_{mi}^{n+1}=V_{pfi}G_{fi}P_{fi}^{n}$$

(3-25)

For matrix

$$\left[-a_3F_{mi-1/2}\right]P_{mi-1}^{n+1}+\left[a_3F_{mi+1/2}+a_3F_{mi-1/2}+\lambda\Delta xA\Delta tH+V_{pmi}G_{mi}\right]P_{mi}^{n+1}+\left[-a_3F_{mi+1/2}\right]P_{mi+1}^{n+1}$$
$$-\lambda\Delta xA\Delta tHP_{fi}^{n+1}=V_{pmi}G_{mi}P_{mi}^{n}$$

(3-26)

i = N-1

For Fracture

$$\left[-a_4F_{fi-1/2}\right]P_{fi-1}^{n+1}+\left[2a_4F_{fi+1/2}+a_4F_{fi-1/2}+\lambda\Delta xA\Delta tH+V_{pfi}G_{fi}\right]P_{fi}^{n+1}+\left[-2a_4F_{fi+1/2}\right]P_{fi+1}^{n+1}$$
$$-\lambda\Delta xA\Delta tHP_{mi}^{n+1}=V_{pfi}G_{fi}P_{fi}^{n}$$

(3-27)

For matrix

$$\left[-a_3F_{mi-1/2}\right]P_{mi-1}^{n+1}+\left[2a_3F_{mi+1/2}+a_3F_{mi-1/2}+\lambda\Delta xA\Delta tH+V_{pmi}G_{mi}\right]P_{mi}^{n+1}+\left[-2a_3F_{mi+1/2}\right]P_{mi+1}^{n+1}$$
$$-\lambda\Delta xA\Delta tHP_{fi}^{n+1}=V_{pmi}G_{mi}P_{mi}^{n}$$

(3-28)

Cell i = N (Downstream cell):

$$\left[-a_5F_{mi-1/2}\right]P_{mi-1}^{n+1}+\left[-a_6F_{fi-1/2}\right]P_{fi-1}^{n+1}+\left[a_5F_{mi-1/2}+-a_6F_{fi-1/2}+V_dG_i\right]P_i^{n+1}+=V_dGP_i^{n}$$

(3-29)

Where

$$a_1=\frac{2k_mA_m\Delta t}{CF\Delta x}$$

$$a_2 = \frac{2k_f A_f \Delta t}{CF\Delta x}$$

$$a_3 = \frac{k_m A_m \Delta t}{CF\Delta x}$$

$$a_4 = \frac{k_f A_f \Delta t}{CF\Delta x}$$

$$a_5 = \frac{2k_m A_m \Delta t}{CF\Delta x}$$

$$a_6 = \frac{2k_f A_f \Delta t}{CF\Delta x}$$

$$V_{pm} = \phi_m A_m \Delta x$$

$$V_{pf} = \phi_f A_f \Delta x$$

A_m = Cross section area of the matrix of the core.

A_f = Cross section area of the fracture of the core.

3.4.1 Finite difference equation for two dimensional

After applying the boundary conditions, the finite difference equations are given as:

Cell i = 1, j (Upstream cell):

$$\left[-hk_m F_{mi,j-1/2}\right]P^{n+1}_{mi,j-1} + \left[-hk_f F_{fi,j-1/2}\right]P^{n+1}_{fi,j-1} +$$
$$\left[\begin{array}{l} hk_m F_{mi,j-1/2} + hk_m\left(\dfrac{2\Delta\psi}{\Delta\phi}\right)F_{mi,j} + hk_m F_{mi,j+1/2} + hk_f F_{fi,j-1/2} + hk_f\left(\dfrac{2\Delta\psi}{\Delta\phi}\right)F_{fi,j} \\ + hk_f F_{fi,j+1/2} + \left(\dfrac{CFV_{pi,j}G_{i,j}}{\Delta t}\right) \end{array}\right]P^{n+1}_{i,j} +$$
$$\left[-hk_m F_{mi,j+1/2}\right]P^{n+1}_{mi,j+1} + \left[-hk_f F_{fi,j+1/2}\right]P^{n+1}_{fi,j+1} + \left(hk_m\left(\frac{-2\Delta\psi}{\Delta\phi}\right)F_{mi,j}\right)P^{n+1}_{mi+1,j} + \left(hk_f\left(\frac{-2\Delta\psi}{\Delta\phi}\right)F_{fi,j}\right)P^{n+1}_{fi+1,j}$$
$$= \left(\frac{CFV_{pi,j}G_{i,j}}{\Delta t}\right)P^{n}_{i,j}$$

(3-30)

Cell i = 2 to N-1, j (Core Sample):

i = 2, j

For fracture

$$\begin{aligned}
&\left[hk_f\left(\frac{-2\Delta\psi}{\Delta\phi}\right)F_{fi-1/2,j}\right]P^{n+1}_{fi_1,j}+\left[hk_f\left(\frac{-\Delta\phi}{\Delta\psi}\right)F_{fi,j-1/2}\right]P^{n+1}_{fi,j-1}+\\
&\left[\begin{array}{l}hk_f\left(\frac{2\Delta\psi}{\Delta\phi}\right)F_{fi-1/2,j}+hk_f\left(\frac{\Delta\phi}{\Delta\psi}\right)F_{fi,j-1/2}+hk_f\left(\frac{\Delta\psi}{\Delta\phi}\right)F_{fi+1/2,j}\\+hk_f\left(\frac{\Delta\phi}{\Delta\psi}\right)F_{fi,j+1/2}+\left(\frac{CFV_{pi,j}G_{fi,j}}{\Delta t}\right)+hA_{i,j}\lambda H_{mi,j}\end{array}\right]P^{n+1}_{fi,j}+\\
&\left[hk_f\left(\frac{-\Delta\phi}{\Delta\psi}\right)F_{fi,j+1/2}\right]P^{n+1}_{fi,j+1}+\left(hk_f\left(\frac{-\Delta\psi}{\Delta\phi}\right)F_{fi+1/2,j}\right)P^{n+1}_{fi+1,j}-hA_{i,j}\lambda H_{mi,j}P^{n+1}_{mi,j}\\
&=\left(\frac{CFV_{pi,j}G_{fi,j}}{\Delta t}\right)P^{n}_{fi,j}
\end{aligned}\tag{3-31}$$

For matrix

$$\begin{aligned}
&\left[hk_m\left(\frac{-2\Delta\psi}{\Delta\phi}\right)F_{mi-1/2,j}\right]P^{n+1}_{mi_1,j}+\left[hk_m\left(\frac{-\Delta\phi}{\Delta\psi}\right)F_{mi,j-1/2}\right]P^{n+1}_{mi,j-1}+\\
&\left[\begin{array}{l}hk_m\left(\frac{2\Delta\psi}{\Delta\phi}\right)F_{mi-1/2,j}+hk_m\left(\frac{\Delta\phi}{\Delta\psi}\right)F_{mi,j-1/2}+hk_m\left(\frac{\Delta\psi}{\Delta\phi}\right)F_{mi+1/2,j}\\+hk_m\left(\frac{\Delta\phi}{\Delta\psi}\right)F_{mi,j+1/2}+\left(\frac{CFV_{pi,j}G_{mi,j}}{\Delta t}\right)+hA_{i,j}\lambda H_{mi,j}\end{array}\right]P^{n+1}_{mi,j}+\\
&\left[hk_m\left(\frac{-\Delta\phi}{\Delta\psi}\right)F_{mi,j+1/2}\right]P^{n+1}_{mi,j+1}+\left(hk_m\left(\frac{-\Delta\psi}{\Delta\phi}\right)F_{mi+1/2,j}\right)P^{n+1}_{mi+1,j}-hA_{i,j}\lambda H_{mi,j}P^{n+1}_{fi,j}\\
&=\left(\frac{CFV_{pi,j}G_{mi,j}}{\Delta t}\right)P^{n}_{mi,j}
\end{aligned}\tag{3-32}$$

i = 3 to N-2, j

For fracture

$$\begin{aligned}
&\left[hk_f\left(\frac{-\Delta\psi}{\Delta\phi}\right)F_{fi-1/2,j}\right]P^{n+1}_{fi_1,j}+\left[hk_f\left(\frac{-\Delta\phi}{\Delta\psi}\right)F_{fi,j-1/2}\right]P^{n+1}_{fi,j-1}+\\
&\left[\begin{array}{l}hk_f\left(\frac{\Delta\psi}{\Delta\phi}\right)F_{fi-1/2,j}+hk_f\left(\frac{\Delta\phi}{\Delta\psi}\right)F_{fi,j-1/2}+hk_f\left(\frac{\Delta\psi}{\Delta\phi}\right)F_{fi+1/2,j}\\+hk_f\left(\frac{\Delta\phi}{\Delta\psi}\right)F_{fi,j+1/2}+\left(\frac{CFV_{pi,j}G_{fi,j}}{\Delta t}\right)+hA_{i,j}\lambda H_{mi,j}\end{array}\right]P^{n+1}_{fi,j}+\\
&\left[hk_f\left(\frac{-\Delta\phi}{\Delta\psi}\right)F_{fi,j+1/2}\right]P^{n+1}_{fi,j+1}+\left(hk_f\left(\frac{-\Delta\psi}{\Delta\phi}\right)F_{fi+1/2,j}\right)P^{n+1}_{fi+1,j}-hA_{i,j}\lambda H_{mi,j}P^{n+1}_{mi,j}\\
&=\left(\frac{CFV_{pi,j}G_{fi,j}}{\Delta t}\right)P^{n}_{fi,j}
\end{aligned}\tag{3-33}$$

For matrix

$$\begin{aligned}
&\left[hk_m\left(\frac{-\Delta\psi}{\Delta\phi}\right)F_{mi-1/2,j}\right]P^{n+1}_{mi_1,j}+\left[hk_m\left(\frac{-\Delta\phi}{\Delta\psi}\right)F_{mi,j-1/2}\right]P^{n+1}_{mi,j-1}+\\
&\left[\begin{array}{l}hk_m\left(\frac{\Delta\psi}{\Delta\phi}\right)F_{mi-1/2,j}+hk_m\left(\frac{\Delta\phi}{\Delta\psi}\right)F_{mi,j-1/2}+hk_m\left(\frac{\Delta\psi}{\Delta\phi}\right)F_{mi+1/2,j}\\+hk_m\left(\frac{\Delta\phi}{\Delta\psi}\right)F_{mi,j+1/2}+\left(\frac{CFV_{pi,j}G_{mi,j}}{\Delta t}\right)+hA_{i,j}\lambda H_{mi,j}\end{array}\right]P^{n+1}_{mi,j}+\\
&\left[hk_m\left(\frac{-\Delta\phi}{\Delta\psi}\right)F_{mi,j+1/2}\right]P^{n+1}_{mi,j+1}+\left(hk_m\left(\frac{-\Delta\psi}{\Delta\phi}\right)F_{mi+1/2,j}\right)P^{n+1}_{mi+1,j}-hA_{i,j}\lambda H_{mi,j}P^{n+1}_{fi,j}\\
&=\left(\frac{CFV_{pi,j}G_{mi,j}}{\Delta t}\right)P^{n}_{mi,j}
\end{aligned}\tag{3-34}$$

i = N-1, j

For fracture

$$\left[hk_f\left(\frac{-\Delta\psi}{\Delta\phi}\right)F_{fi-1/2,j}\right]P^{n+1}_{fi\_1,j}+\left[hk_f\left(\frac{-\Delta\phi}{\Delta\psi}\right)F_{fi,j-1/2}\right]P^{n+1}_{fi,j-1}+$$
$$\left[\begin{array}{l}hk_f\left(\frac{\Delta\psi}{\Delta\phi}\right)F_{fi-1/2,j}+hk_f\left(\frac{\Delta\phi}{\Delta\psi}\right)F_{fi,j-1/2}+hk_f\left(\frac{2\Delta\psi}{\Delta\phi}\right)F_{fi+1/2,j}\\+hk_f\left(\frac{\Delta\phi}{\Delta\psi}\right)F_{fi,j+1/2}+\left(\frac{CFV_{pi,j}G_{fi,j}}{\Delta t}\right)+hA_{i,j}\lambda H_{mi,j}\end{array}\right]P^{n+1}_{fi,j}+ \quad (3\text{-}35)$$
$$\left[hk_f\left(\frac{-\Delta\phi}{\Delta\psi}\right)F_{fi,j+1/2}\right]P^{n+1}_{fi,j+1}+\left(hk_f\left(\frac{-2\Delta\psi}{\Delta\phi}\right)F_{fi+1/2,j}\right)P^{n+1}_{fi+1,j}-hA_{i,j}\lambda H_{mi,j}P^{n+1}_{mi,j}$$
$$=\left(\frac{CFV_{pi,j}G_{fi,j}}{\Delta t}\right)P^{n}_{fi,j}$$

For matrix

$$\left[hk_m\left(\frac{-\Delta\psi}{\Delta\phi}\right)F_{mi-1/2,j}\right]P^{n+1}_{mi\_1,j}+\left[hk_m\left(\frac{-\Delta\phi}{\Delta\psi}\right)F_{mi,j-1/2}\right]P^{n+1}_{mi,j-1}+$$
$$\left[\begin{array}{l}hk_m\left(\frac{\Delta\psi}{\Delta\phi}\right)F_{mi-1/2,j}+hk_m\left(\frac{\Delta\phi}{\Delta\psi}\right)F_{mi,j-1/2}+hk_m\left(\frac{2\Delta\psi}{\Delta\phi}\right)F_{mi+1/2,j}\\+hk_m\left(\frac{\Delta\phi}{\Delta\psi}\right)F_{mi,j+1/2}+\left(\frac{CFV_{pi,j}G_{mi,j}}{\Delta t}\right)+hA_{i,j}\lambda H_{mi,j}\end{array}\right]P^{n+1}_{mi,j}+ \quad (3\text{-}36)$$
$$\left[hk_m\left(\frac{-\Delta\phi}{\Delta\psi}\right)F_{mi,j+1/2}\right]P^{n+1}_{mi,j+1}+\left(hk_m\left(\frac{-2\Delta\psi}{\Delta\phi}\right)F_{mi+1/2,j}\right)P^{n+1}_{mi+1,j}-hA_{i,j}\lambda H_{mi,j}P^{n+1}_{fi,j}$$
$$=\left(\frac{CFV_{pi,j}G_{mi,j}}{\Delta t}\right)P^{n}_{mi,j}$$

Cell i = N, j (Downstream cell):

$$\left[hk_m\left(\frac{-2\Delta\psi}{\Delta\phi}\right)F_{mi-1/2,j}\right]P^{n+1}_{mi\_1,j}+\left[hk_f\left(\frac{-2\Delta\psi}{\Delta\phi}\right)F_{fi-1/2,j}\right]P^{n+1}_{fi\_1,j}+\left[-hk_mF_{mi,j-1/2}\right]P^{n+1}_{mi,j-1}+\left[-hk_fF_{fi,j-1/2}\right]P^{n+1}_{fi,j-1}+$$
$$\left[\begin{array}{l}hk_m\left(\frac{2\Delta\psi}{\Delta\phi}\right)F_{mi-1/2,j}+hk_mF_{mi,j-1/2}+hk_mF_{mi,j+1/2}+hk_f\left(\frac{2\Delta\psi}{\Delta\phi}\right)F_{fi-1/2,j}+hk_fF_{fi,j-1/2}\\+hk_fF_{fi,j+1/2}+\left(\frac{CFV_{pi,j}G_{i,j}}{\Delta t}\right)\end{array}\right]P^{n+1}_{i,j}+$$
$$\left[-hk_mF_{mi,j+1/2}\right]P^{n+1}_{mi,j+1}+\left[-hk_fF_{fi,j+1/2}\right]P^{n+1}_{fi,j+1}=\left(\frac{CFV_{pi,j}G_{i,j}}{\Delta t}\right)P^{n}_{i,j}$$

(3-37)

$F_{i,j}$ is the Harmonic Mean of the values of the function F. For example, at the following cells (i, j-1) and (i, j), it is given by

$$F_{i,j-1/2}=\frac{2F_{i,j-1}F_{i,j}}{F_{i,j-1}+F_{i,j}} \tag{3-38}$$

The area of the grid cell is estimated by using the following equations:

$$A_{i,j}=\frac{1}{2}\left|\begin{array}{l}(X_1-X_2)(Y_1+Y_2)+(X_2-X_3)(Y_2+Y_3)\\+(X_3-X_4)(Y_3+Y_4)+(X_4-X_1)(Y_4+Y_1)\end{array}\right| \tag{3-39}$$

Thus the pore volume of the grid cell can be given as

$$V_{Pi,j}=A_{i,j}h\varphi \tag{3-40}$$

CHAPTER 4

THE COMPUTER MODEL

Based on the developed numerical solution, computer program was developed that can simulate the pressure pulse decay experiments and generate the pressure pulse decay data with respect to time.

4.1 Determination of the physical properties of Nitrogen

Because Nitrogen has been used as the flowing compressible fluid for the pressure pulse decay experiments, it is essential to estimate the physical properties that are functions of pressure and temperature. These properties are gas compressibility factor (z) and gas viscosity (μ).

The equations which are used in the computer program for determining Nitrogen properties are given in the following section.

4.1.1 Gas Viscosity (μ_g)

The viscosity of Nitrogen at temperature close to 25^{O}C can be calculated from the following equation [3]

$$\mu_{N_2}[T,P] = \mu_{N_2}[T,1] - 0.12474 + 0.123688P + 1.05452\times10^{-3}P^2 - 1.5052\times10^{-6}P^3 \quad (4\text{-}1)$$

Where $\mu_{N2}[T,1]$ is the viscosity of Nitrogen at one atmosphere pressure and can be obtained from the following equation [3]

$$\mu_{N_2}[T,1] = \frac{13.85T^{1.5}}{T+102} \quad (4\text{-}2)$$

The pressure in equation (4.1) is in atmosphere and the temperature in equation (4.2) is in degrees Kelvin.

4.1.2 Gas compressibility factor (z)

For an ideal gas, gas compressibility factor is equal to 1.0, but for real gas, gas compressibility factor is also included in the fluid flow equations. The values of z-factor for Nitrogen were obtained as a function of pressure by fitting a 3^{rd} degree polynomial to the data given in API RP-40[3] for a temperature of 25^{O} C.

$$z = 1.0 - 0.196929 \times 10^{-4} P + 0.150321 \times 10^{-7} P^2 - 0.67322510^{-12} P^3 \qquad (4\text{-}3)$$

The values of pressure used in equation (4.3) are in psia.

4.1.3 The compressibility of gas (c_g)

Equation (4.4) is used for calculating the compressibility of gas (c_g)

$$\mathrm{c_g} = \frac{1}{P} - \frac{1}{z}\frac{\partial z}{\partial P} \qquad (4\text{-}4)$$

Where $\left(\frac{\partial z}{\partial P}\right)$ is obtained by differentiating equation (4.3). The pressure in equation (4.4) is in psia.

4.2 Determination of gas slippage

The values of klinkenberg constant (b) have been calculated from the available correlation. For estimating of klinkenberg constant (b), Jones[15] correlation has been used

$$b = 6.9k^{-0.36} \tag{4-5}$$

Where

k = Permeability (md).

4.3 Nonlinear regression

The computer program, which is developed based on the mathematical model, was used to analyze the pressure pulse decay data using nonlinear regression technique to estimate the permeability. A brief overview of the nonlinear regression is given below.

Nonlinear regression is a powerful method for analyzing data described by nonlinear model. A nonlinear regression model is given as

$$Y_i = f(x_i, \theta) + \varepsilon_i \quad \text{i} = 1, 2 \ldots \text{n} \tag{4-6}$$

Where

Y = dependent variable.

x = independent variable.

θ = unknown parameters.

ε = normal errors.

$f(x, \theta)$ = function of unknown parameters.

To determine the unknown parameters "θ", the method of least square is used by minimizing the residual of model, i.e.

$$e_i(\theta) = Y_i - f(x_i, \theta) \tag{4-7}$$

Equation (4.8) shows the value of "θ" that minimize the sum of squares of the deviations of the observations form the regression model,

$$S = \sum_{i=1}^{n} (e_i(\theta))^2 = \sum_{i=1}^{n} [Y_i - f(x_i, \theta)]^2 \tag{4-8}$$

The estimation of "θ" from the least square say "$\hat{\theta}$" must satisfy,

$$\frac{\partial S}{\partial \theta} = \sum_{i=1}^{n} -2[Y_i - f(x_i, \theta)] \frac{\partial f(x_i, \theta)}{\partial \theta} \tag{4-9}$$

When this partial derivation is set equal to zero and parameters "θ" are replaced by the least squares estimations "$\hat{\theta}$", we get the normal equation as follows,

$$\sum_{i=1}^{n} Y_i \left(\frac{\partial f(x_i, \theta)}{\partial \theta} \right)_{\theta=\hat{\theta}} - \sum_{i=1}^{n} f(x_i, \theta) \left(\frac{\partial f(x_i, \theta)}{\partial \theta} \right)_{\theta=\hat{\theta}} = 0 \tag{4-10}$$

In this study, pressure drop, ΔP, and upstream pressure, P_u, are the dependent variable while time, t, is the independent variable. The unknown parameters are matrix permeability, k_m, fracture permeability, k_f, and interporosity flow parameter , λ.

CHAPTER 5

EXPERIMENTAL EQUIPMENT AND PROCEDURE

An experimental setup was constructed to perform pressure pulse decay experiments for determining the matrix and fracture permeabilites. Whole cores used in this study were selected from a low permeability reservoir. Furthermore, Nitrogen was used as the flowing fluid. The experimental setup used for pressure pulse decay technique is shown in Figure 5.1.

5.1 Experimental Apparatus

In this part, the components of the experimental setup for the pressure pulse decay technique are described.

5.1.1 Core holder

The core holder (Figure 5.2) used in the experiments to hold the whole core sample during the test is constructed of stainless steel. The core holder can accommodate 1 ft long and 4 inches diameter whole core samples. The whole core

samples used in the pressure pulse decay test are 4.7 inches long and 4 inches in diameter. They are mounted inside the rubber sleeve and then subjected to overburden pressure of about 1000 psig. Two mesh screens of equal width, covering a subtended angle (θ), are placed on the opposite ends of the core sample parallel to the axis of the core and running the full length. Two aluminum spacers are placed at the ends of the core. The center of each spacer has "L" shaped hole. The whole assembly is mounted within the core holder. The core holder has a build-in end plug in the closed end. There is a movable end plug on the other end to accommodate variable lengths of the core samples. The fluid which is used in the experiment enters the core holder through a stainless steel tube which is connected to the movable end plug. Then, the fluid enters the spacer through the "L" shaped hole. The fluid leaves from the opposite side and out of the core holder by using the same way which was used for inlet except that this side is on the other closed end of the core holder.

5.1.2 Upstream and downstream vessels

There are two vessels, one on the upstream side and the other on the downstream side. Each vessel has volume of approximately 250 cc. This volume of the vessels can be

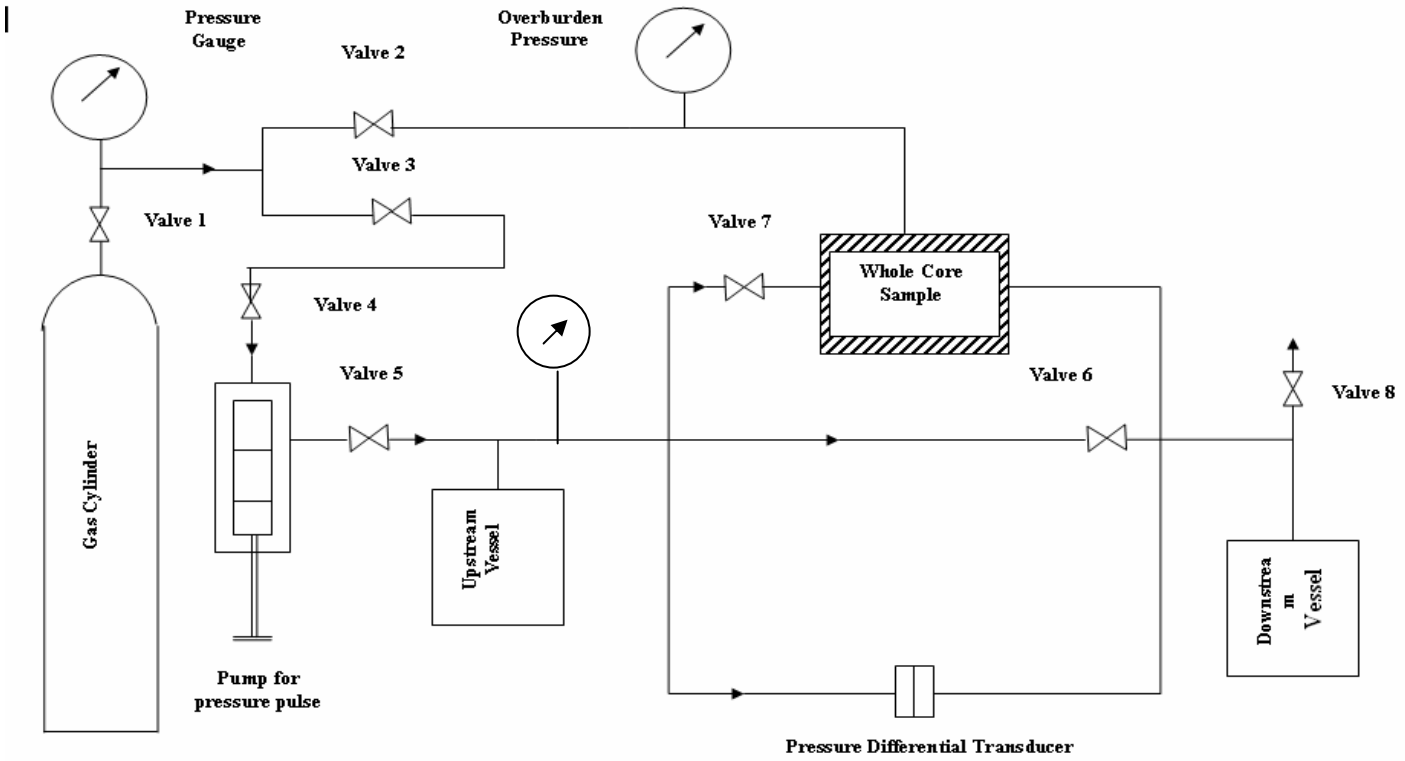

Figure 5-1 Experimental set-up for pressure pulse decay test

decreased by placing any solid material inside it.

5.1.3 Pressure gauges

Pressure gauges and pressure transducers are used to measure the pressure at various positions, for example Nitrogen cylinder pressure, pressure in the upstream and downstream vessels and overburden pressure. For upstream vessel pressure measurement, a pressure transducer of 0-125 psig is used. Also 0-3000 psig gauge is used for overburden pressure. For Nitrogen cylinder 0-4000 psig is used. Pressure gauges with digital displays are used for accurate measurements.

5.1.4 Valves and fittings

As shown in the Figure 5.1, about eight valves are used. These valves and fittings are of the same rating as the tubing is.

5.1.5 Piping

Stainless steel tubing is needed to connect pump, the Nitrogen cylinder, core holder and the upstream and downstream vessels. The size of these tubing is 1/8 inches and can stand a pressure of 2500 psig.

5.1.6 Nitrogen gas cylinder

For supplying enough gas during the experimental runs, a Nitrogen gas cylinder is required. This cylinder contained Nitrogen gas at about 2000 psig. A pressure regulator is used to adjust the pressure from the cylinder according to the requirements of the pressure pulse decay experiments.

5.1.7 Pump for pressure pulse

In the experiment to create a small and controlled pressure pulse a mercury injection hand pump is used. This pump is used to create a pressure pulse of any desired magnitude.

5.1.8 Pressure differential transducers and data acquisition system

During the test, pressure differential transducers are needed to measure the pressure difference across the whole core sample. These transducers are calibrated with their respective digital indicators. The transducers of 12.5 psi and 125 psi are used as per the requirements of the experiments.

The electrical signals sent by the transducers are digitized by a data translation board and sent to a data acquisition software in the computer. This software records the pressure pulse decay with respect to time and displays it graphically on the computer screen and also creates a data file on the hard disk of the computer for future record and analysis.

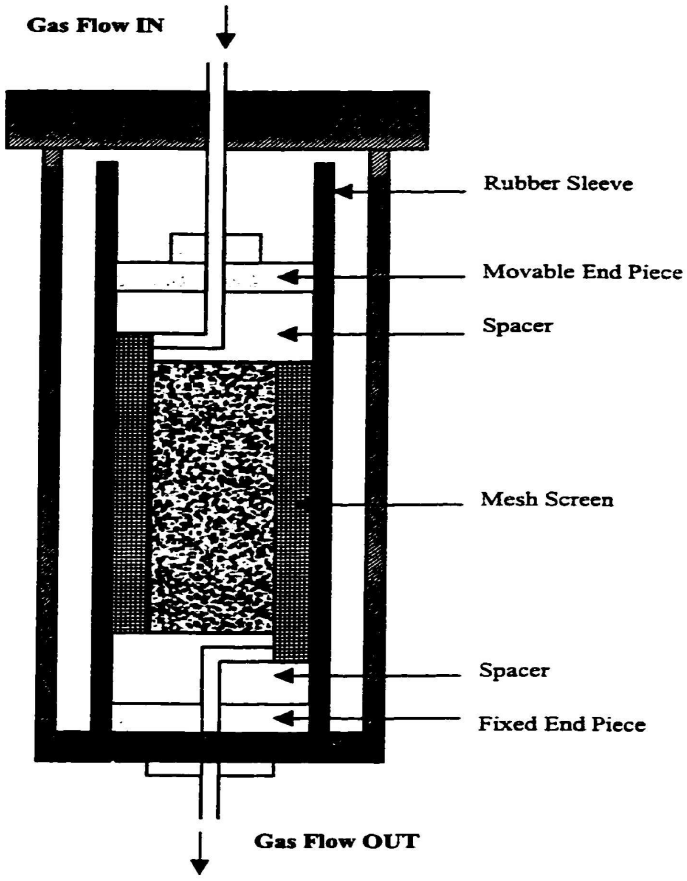

Figure 5-2 Schematic diagram of core holder

5.2 Pre-Experimental Procedures

5.2.1 Temperature

According to Charles' law, as gas expands, its temperature drop. But in the development of the mathematical model, the fluid flow was assumed to be isothermal. Moreover, it is very difficult to accurately determine this variation of temperature with pressure during the test. Therefore, to avoid these problems, the upstream and downstream cells plus the entire tubing network were insulated using glass wool. Furthermore, copper tube bundles which were placed in the vessels minimize the cooling effect of gas due to the gas expansion in the upstream and downstream vessels. Also the temperature variation in the system is reduced due to the high heat capacity of the copper.

5.2.2 Testing and Calibration of the Experimental Setup

Before performing the pressure pulse decay tests, the experimental setup was tested for any leaks. The system was pressurized up to 600 psig and was then left for 24 hours to check for any leak. Soap water bubble tester was used for locating any major leak.

After completing the pressure testing, the system was calibrated to measure the total volume of the upstream and downstream vessels, tubing, valves and joints. By applying Boyle's law, after the expanding of gas from one volume to the other volume, the upstream and downstream volumes were estimated by measuring pressure drop. The same procedure was used to determine the volume of tubing, valves and joints.

5.3 Experimental Procedure:

In this part, summary of procedures for measurements of porosity using Boyle's law gas expansion method and permeability measurements using pressure pulse decay technique are described.

5.3.1 Porosity Measurements

Porosity is defined as the ratio of pore volume to bulk volume of the core sample. The experimental setup used for measuring porosity is shown in Figure 5.3. For measuring porosity, Boyle's law is used. The procedure of the measurement of porosity can be described as:

- Open the Nitrogen gas cylinder while keeping valve 2 close and fill the first volume (V_1).

- Close the Nitrogen gas cylinder valve and wait for the pressure to stabilize. Then, record the initial pressure (P_{ini}).

- Open valve 2 to fill the core sample (V_2). After that, record the final pressure (P_{final}). Finally, release the pressure from the recorded volume 2.

- Repeat the above steps at least three times and then plot initial pressure versus final pressure and calculated the slope.

- Compute the pore volume by using equation 5.1.

$$V_{pore} = V_2 - [(slope - 1) \times V_1] \tag{5-1}$$

- Use equation 5.2 to compute the porosity

$$\phi = \frac{V_{pore}}{V_{bulk}} \tag{5-2}$$

Where

V_1 = plumbing and transfer cell volume

V_2 = core sample and piping volume

V_p = Pore volume of the core sample

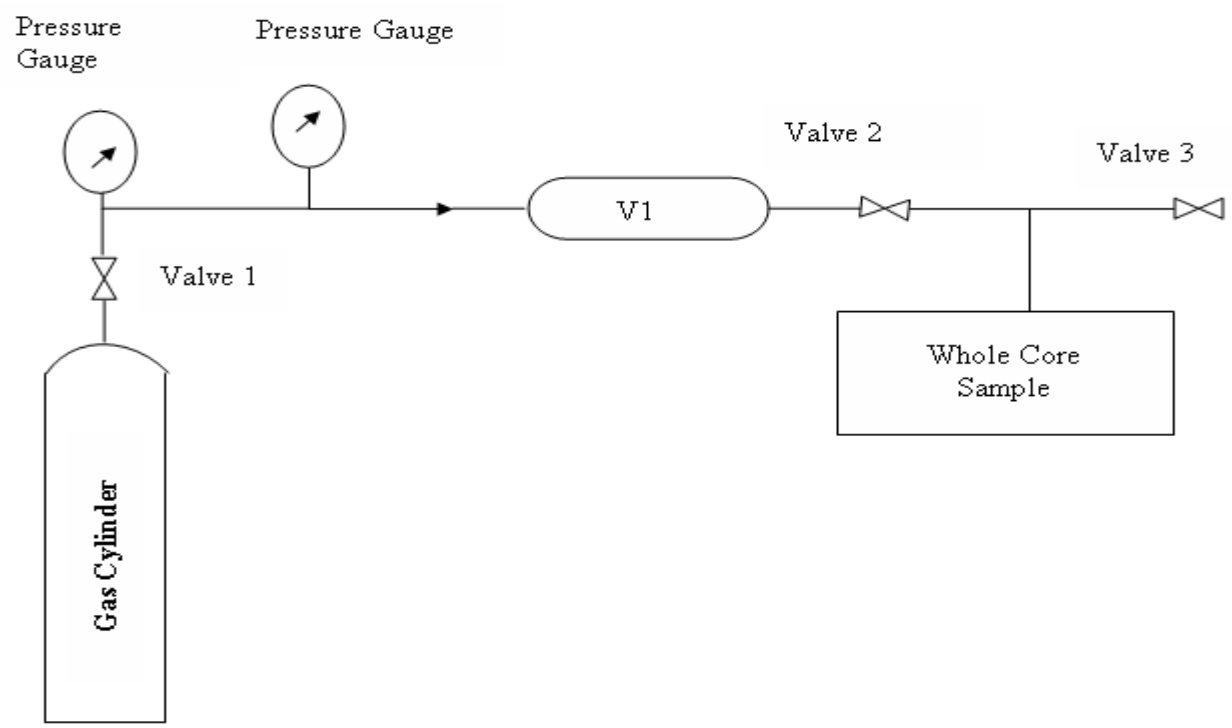

Figure 5-3 Experiment set-up for measuring porosity

5.3.2 Permeability Measurement

The summary of the dimension, porosity and other relevant details of the two core samples are shown in Table 5.1. The procedure to perform the pressure pulse decay experiments is as follows:

- Insert the core sample inside the sleeve and then, place it into the core holder.

- After the placement of the core in the core holder, apply a net overburden pressure of 1000 psig.

- Close valve 8 (Figure 5.1) and pressurize the system to some initial system pressure. Then, allow the pressure to be stabilized for few minutes. During this time valves 6 and 7 should be open. Note that this pressure is the initial downstream pressure.

- Provide the required parameters in the data acquisition program and also provide the required time interval for recording the pressure readings.

- Close valves 6 and 7 and increase the upstream pressure to have some pressure difference between the upstream and downstream vessels. After that, wait for few minutes for the pressure to stabilize.
- Click on start button of the data acquisition program and then open valve 7 to allow the gas to flow through the core sample. The upstream cell pressure and the differential pressure between upstream and downstream cells are recorded as a function of time as shown graphically by the data acquisition program on the computer. The pressure-time data is then analyzed using the developed data analysis computer program to calculate the fracture and matrix permeabilities of the core sample.

Table 5-1 Dimension and Porosity of Whole Core Samples

Sample Number	Length (cm)	Diameter (cm)	Porosity %
CS 1	11.92	10.05	13.56
CS 2	11.58	10.12	12.7

CHAPTER 6

RESULTS AND DISCUSSION

The experimental and simulation results are analyzed, discussed and presented in this chapter. The simulator is used to study the effect of upstream and downstream reservoir volume, matrix permeability/fracture permeability ratio, gas slippage, interporosity flow parameter and the area of fracture on pressure pulse decay curves.

6.2 Comparison of numerical solution and analytical solution

The parameters used to generate the simulation results such as core diameter, core length, upstream and downstream reservoir volume and temperature are listed in Table 6.1. The estimated value of gas slippage is calculated from Equation (4.5).

The developed numerical simulator results are compared with available analytical solution [20]. The results are shown in Figure 6.1. Figure 6.1shows a very small difference between the numerical results and the analytical results.

Table 6-1 The simulator input data

Parameter	Value
Upstream cell volume	3 cc
Downstream cell volume	2 cc
Length of the core sample	5 cm
Temperature	25 ^{o}c
Number of grid cells in X-direction	20
Number of grid cells in Y-direction	1
Matrix permeability	0.00001md
Fracture permeability	10 md
Matrix porosity	4%
Fracture porosity	10%
Area of matrix	4 cm^2
Area of fracture	0.0002 cm^2
Interporosity flow parameter	2.5×10^{-5}

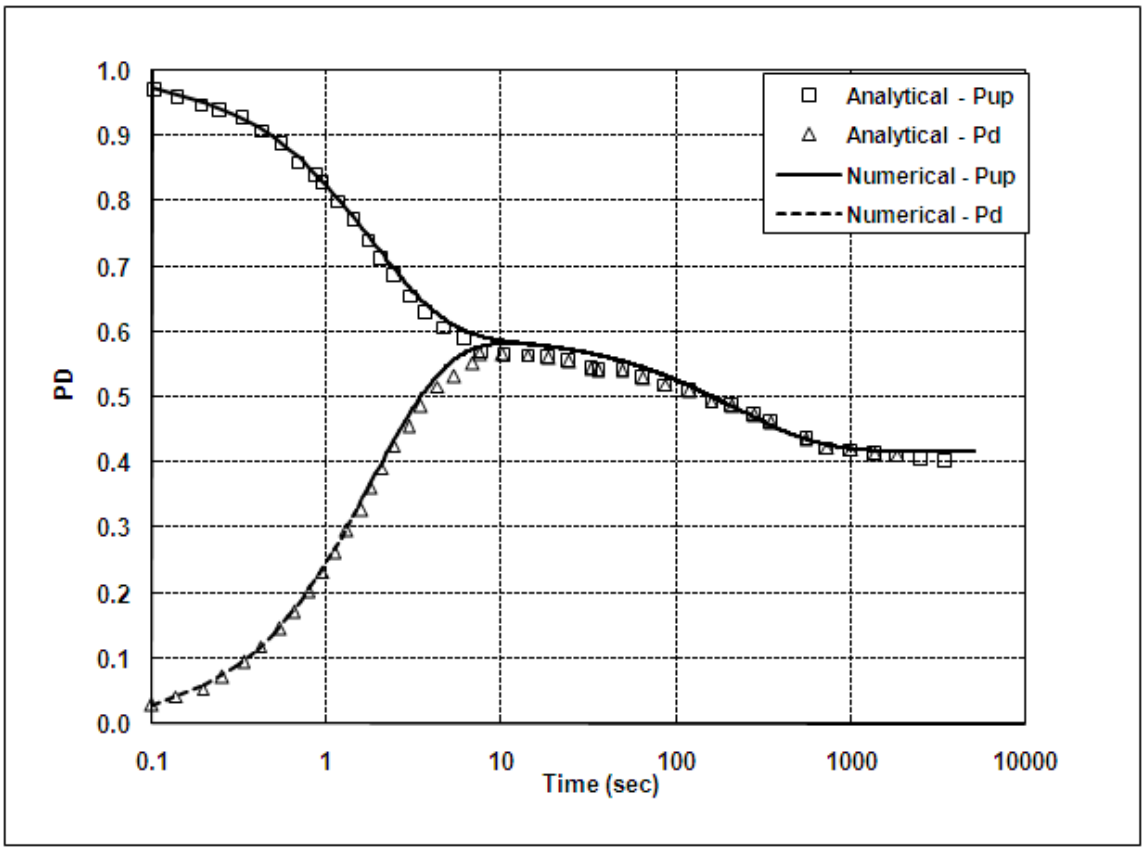

Figure 6-1 Comparison of numerical solution with analytical solution

6.2 Effect of upstream and downstream reservoir volume on pressure pulse decay curves

Several simulation runs were performed to study the effect of upstream and downstream cell volumes on pressure pulse decay (PPD) curves. For matrix permeability ranging from 0.5 to 2 *md* with fracture permeability of 10000 *md*. The values of other parameters such as porosity of the matrix, porosity of the fracture, the temperature and the core samples dimensions used in the generation of simulation are tabulated in Table 6.2. The pressure pulse decay (PPD) curves are plotted as pressure vs. time for the following conditions:

- The pore volume of the core sample is smaller than upstream and downstream reservoir volumes.
- The pore volume of the core sample is equal to the upstream and downstream reservoir volumes.
- Upstream and downstream reservoir volumes are equal 50% of the pore volume of the core sample.
- Upstream and downstream reservoir volumes are equal 20% of the pore volume of the core sample.

In all cases, the volume of upstream reservoir is equal to the downstream reservoir volume.

When gas pulse decay measurements are used for low permeability samples, one or both of the reservoirs is relatively small in volumes[23]. The results of all runs are shown in Figures 6.2 to 6.13. The results indicate that in the first three cases, there is no effect of fracture permeability on pressure pulse decay curves but on case four, the effect of fracture permeability can be seen clearly in the downstream pressure curve.

In case four, gas flows from the upstream cell through the fracture and also the gas flows from upstream cell, downstream cell and fracture through the matrix. Because the matrix permeability is smaller than the fracture permeability, the downstream pressure curve increases at the beginning and then decreases.

Table 6-2 Parameters used in the simulator input data

Core Sample ID	BH3	BH6	BH8
Length of the core sample (H)	7.549 cm	7.615 cm	7.785 cm
Radius of the core sample (R)	3.8 cm	3.8 cm	3.8 cm
Temperature (T)	$25^{\circ}c$	$25^{\circ}c$	$25^{\circ}c$
Porosity of matrix (ϕ_m)	10.6 %	10.7 %	7.1 %
Porosity of fracture (ϕ_f)	80%	80%	80%
Permeability of matrix (k_m)	0.542 md	1.823 md	0.1424 md
Permeability of fracture (k_f)	10000 md	15000 md	10000 md
Interporosity flow (λ)	0.01	0.01	0.01
Area of matrix (A_m)	0.999A	0.999A	0.999A
Area of fracture (A_f)	0.001A	0.001A	0.001A

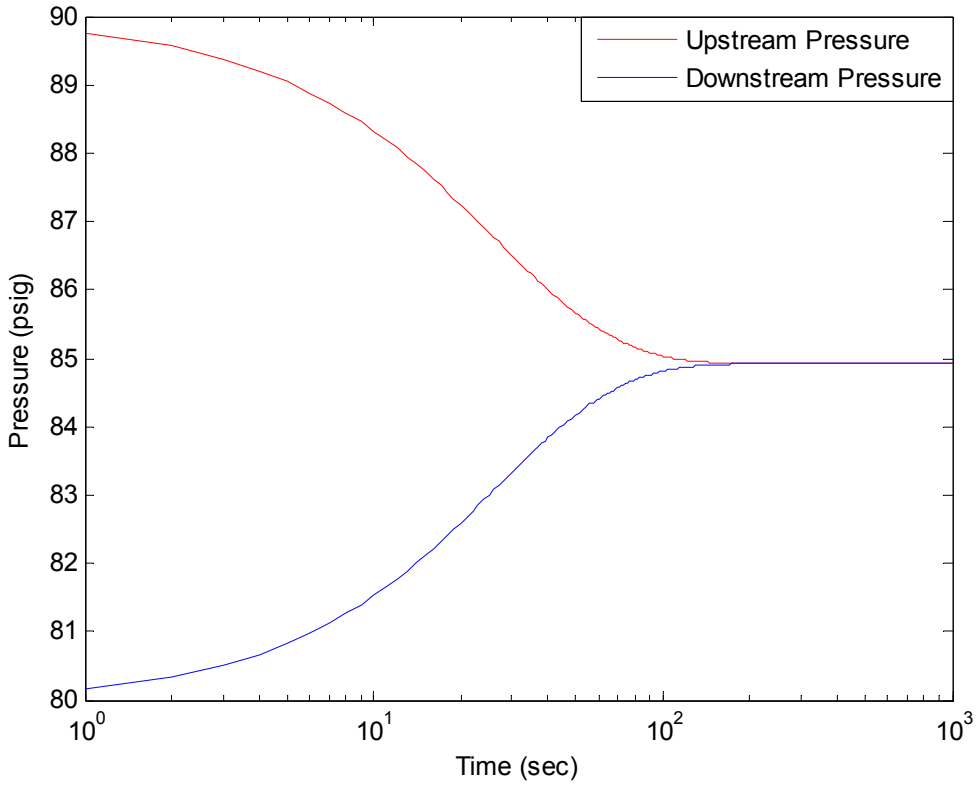

Figure 6-2 Effect of upstream and downstream reservoir volume on PPD curves for core BH3 ($V_u = V_d = 250cc$ & pore volume of the core sample = 9.1cc)

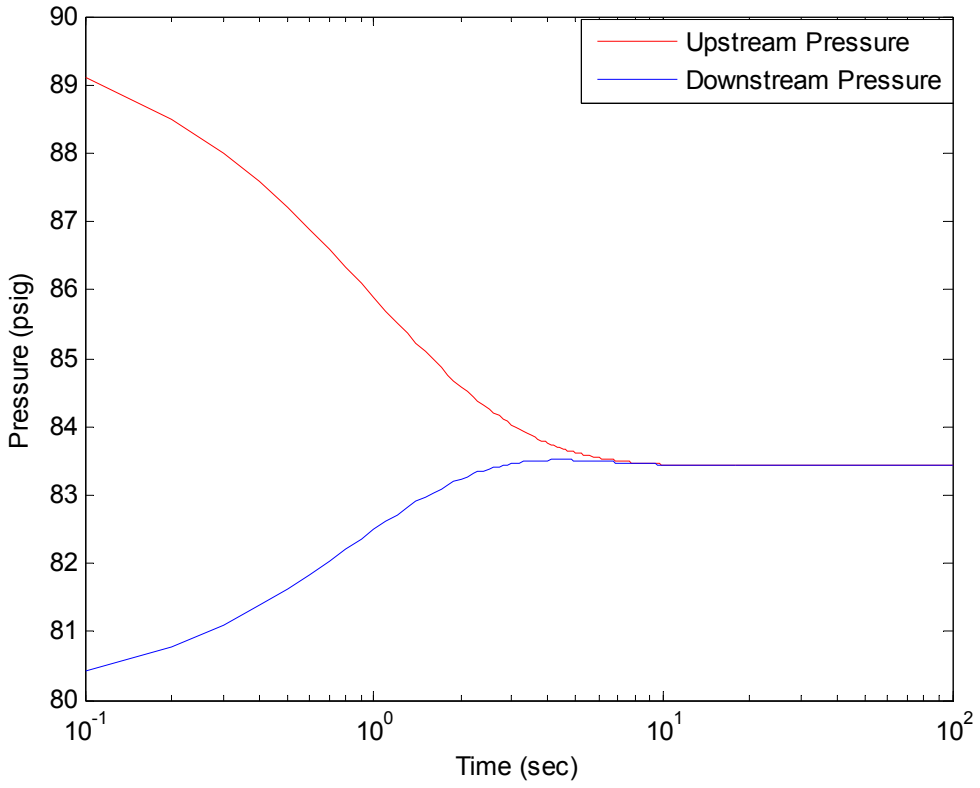

Figure 6-3 Effect of upstream and downstream reservoir volume on PPD curves for core BH3 ($V_u = V_d = 9cc$ & pore volume of the core sample = 9.1cc)

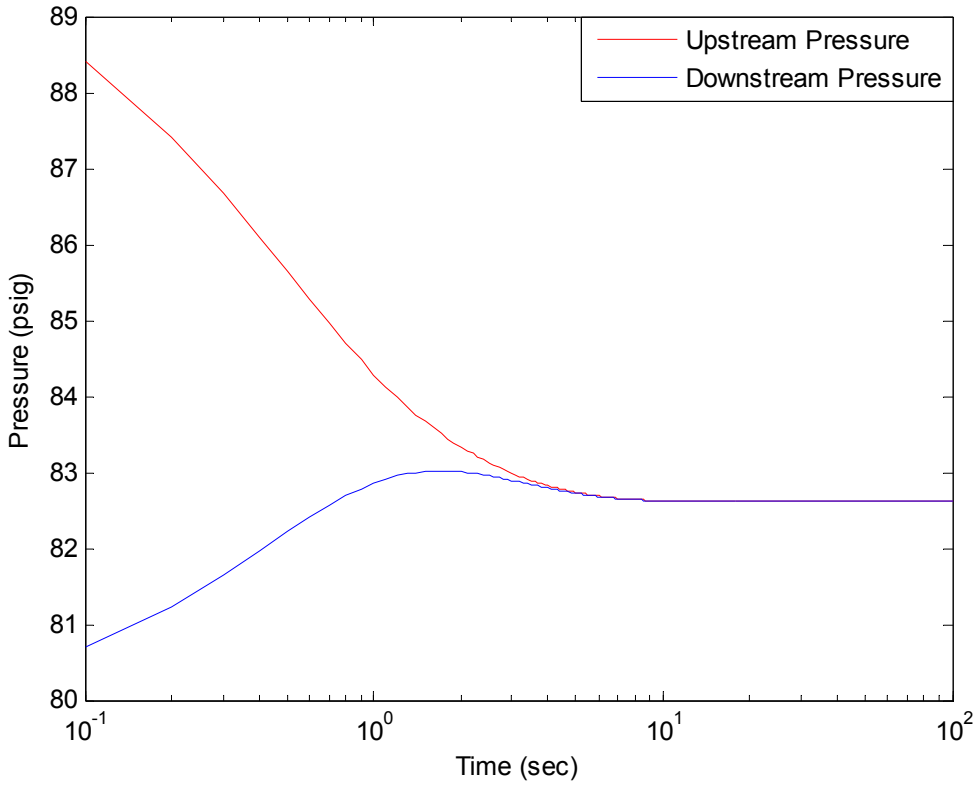

Figure 6-4 Effect of upstream and downstream reservoir volume on PPD curves for core BH3 ($V_u = V_d = 4.5cc$ & pore volume of the core sample = 9.1cc)

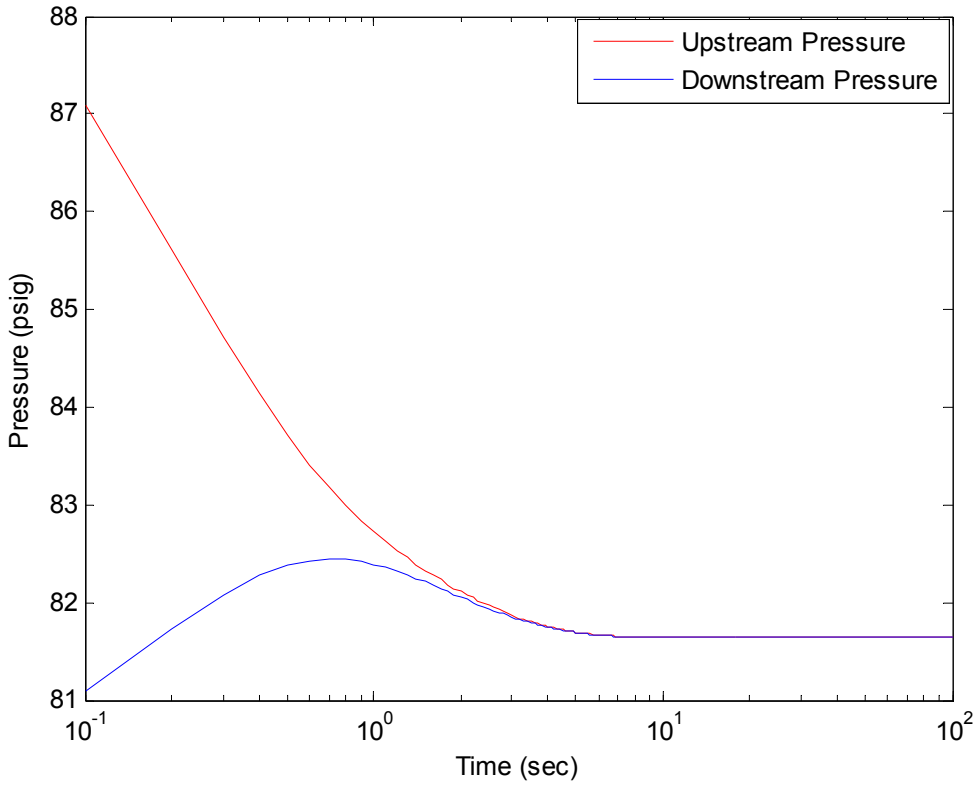

Figure 6-5 Effect of upstream and downstream reservoir volume on PPD curves for core BH3 ($V_u = V_d = 2cc$ & pore volume of the core sample = 9.1cc)

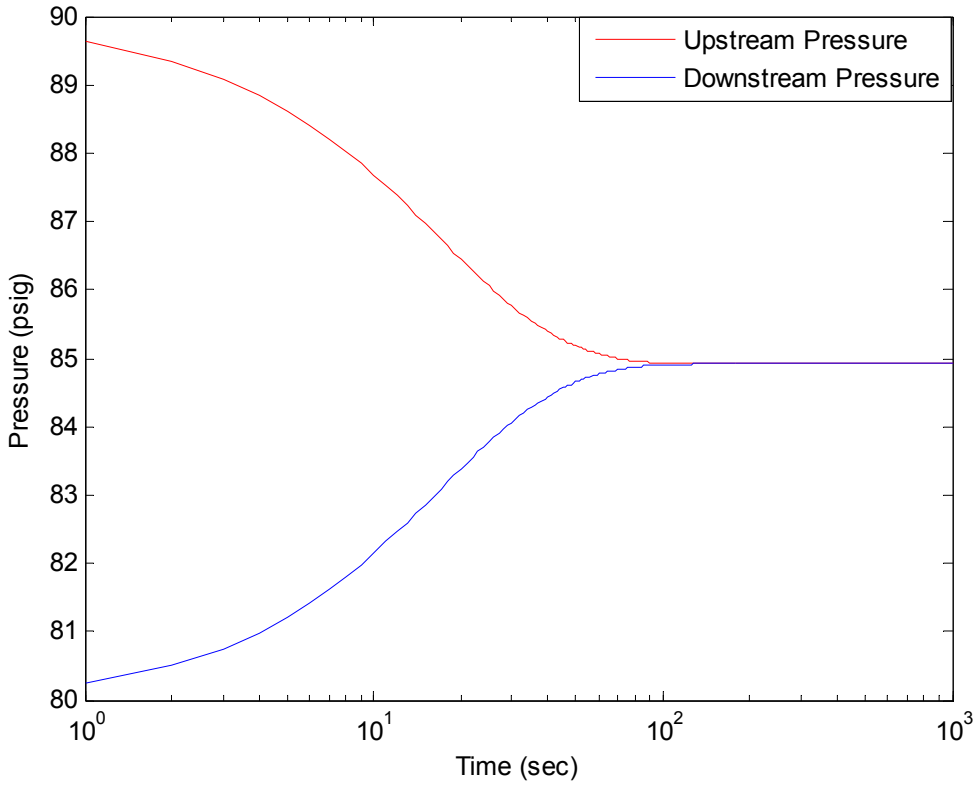

Figure 6-6 Effect of upstream and downstream reservoir volume on PPD curves for core BH6 ($V_u = V_d = 250cc$ & pore volume of the core sample = 9.2cc)

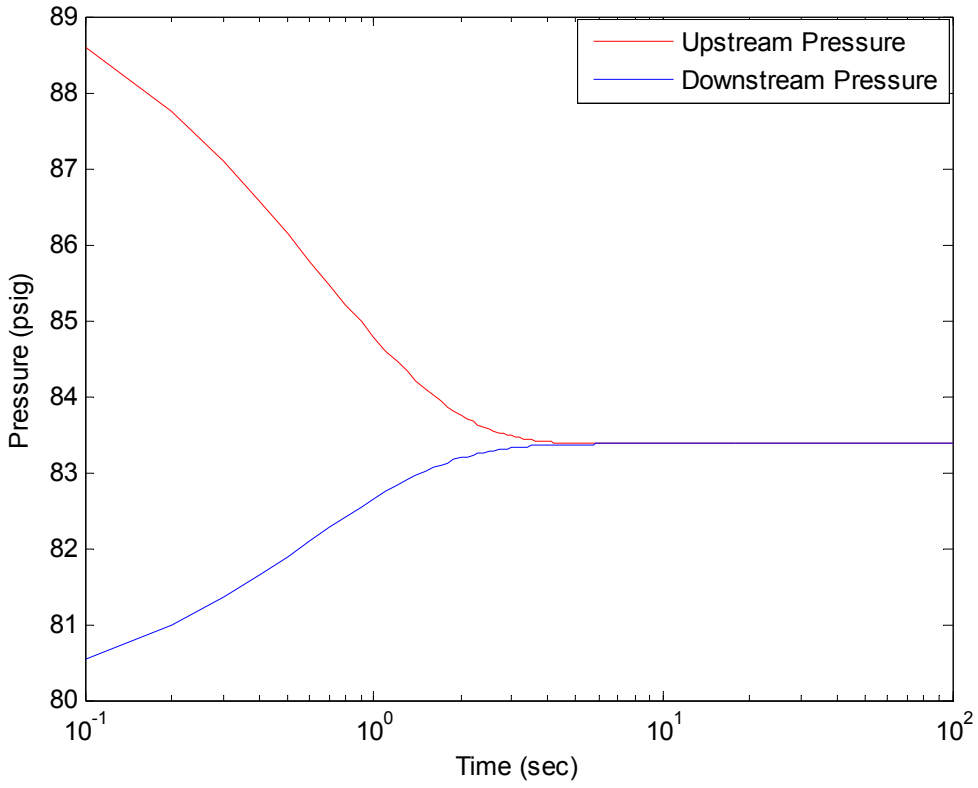

Figure 6-7 Effect of upstream and downstream reservoir volume on PPD curves for core BH6 ($V_u = V_d = 9cc$ & pore volume of the core sample = 9.2cc)

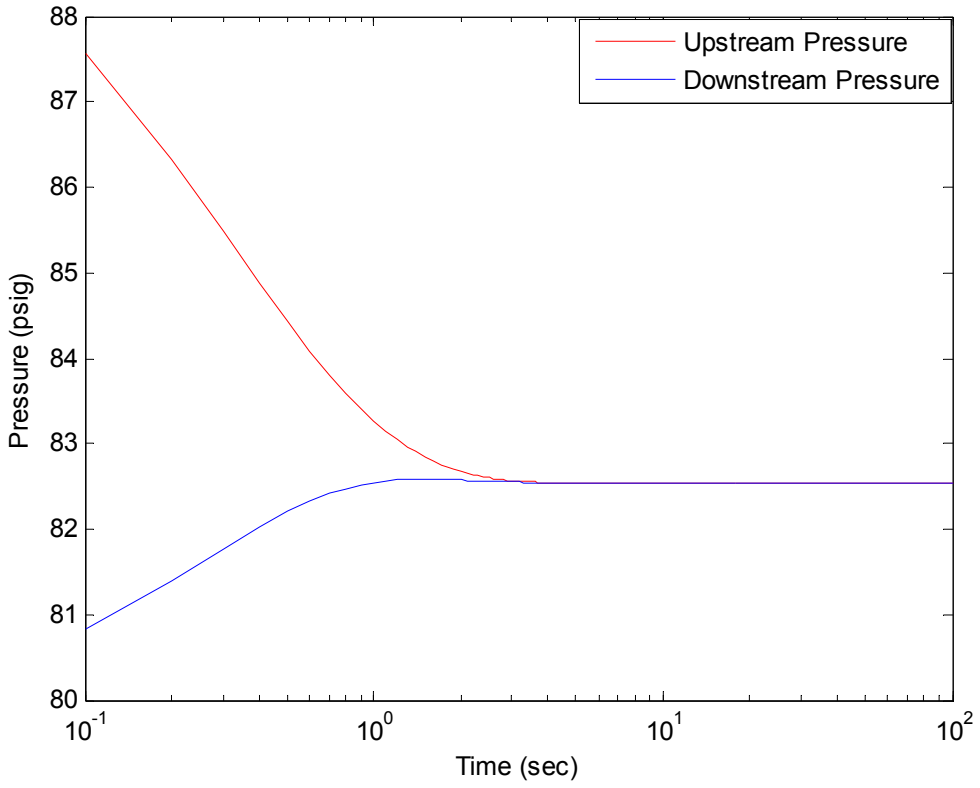

Figure 6-8 Effect of upstream and downstream reservoir volume on PPD curves for core BH6 ($V_u = V_d = 4.5cc$ & pore volume of the core sample = 9.2cc)

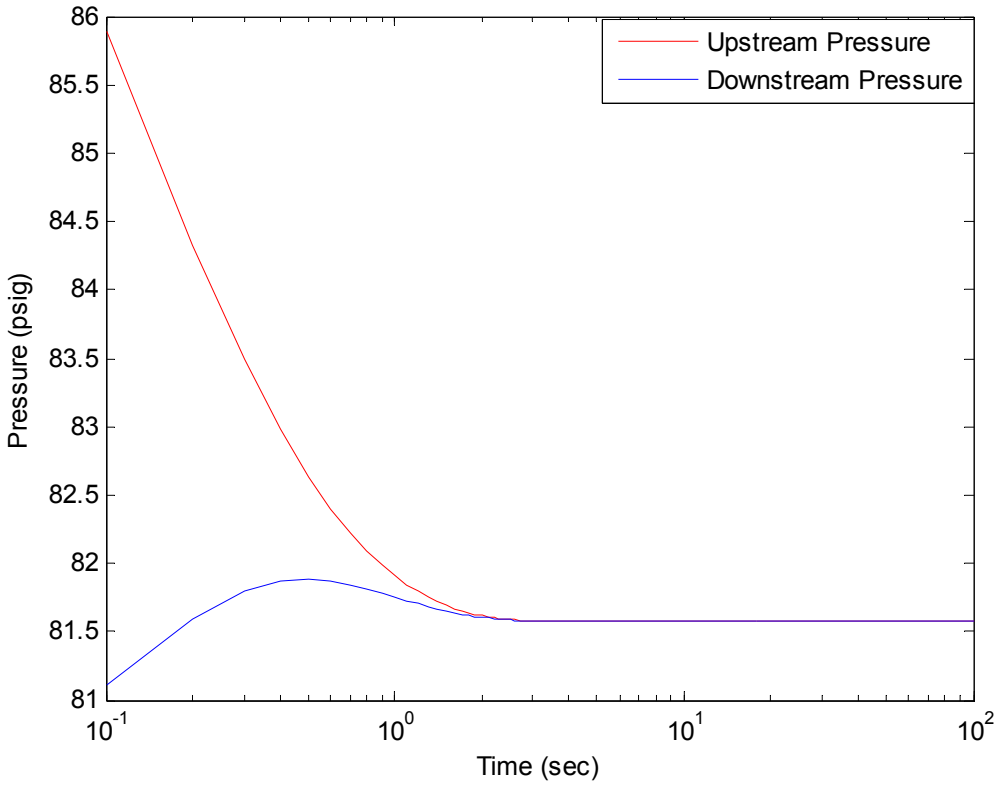

Figure 6-9 Effect of upstream and downstream reservoir volume on PPD curves for core BH6 ($V_u = V_d = 2cc$ & pore volume of the core sample = 9.2cc)

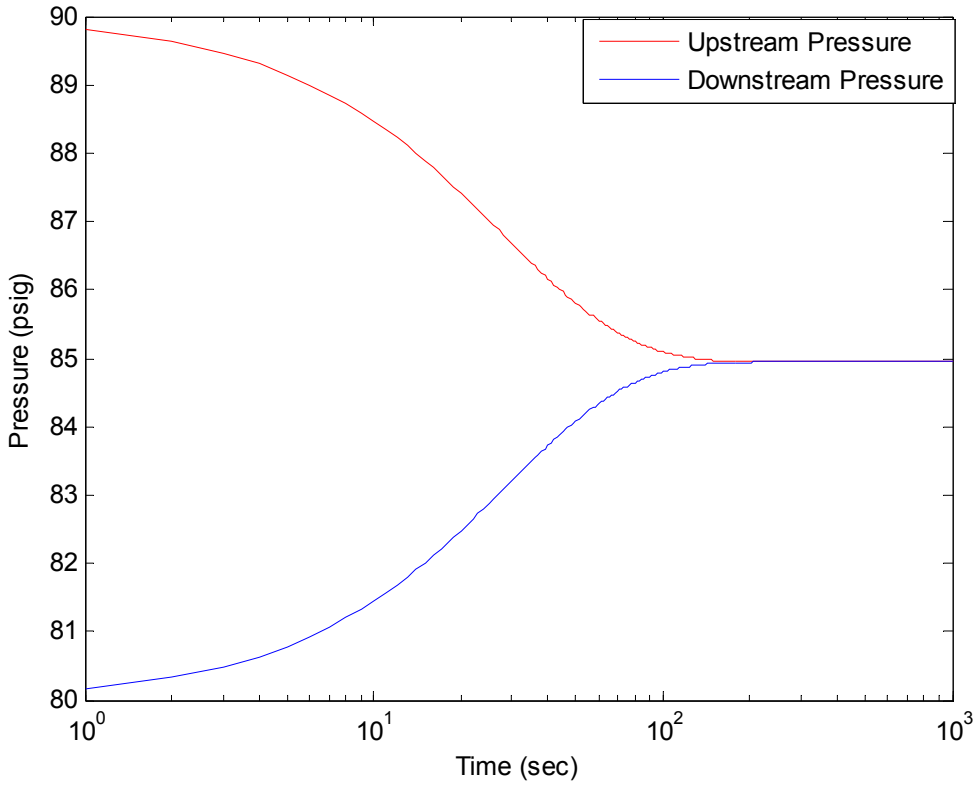

Figure 6-10 Effect of upstream and downstream reservoir volume on PPD curves for BH8 ($V_u = V_d = 250cc$ & pore volume of the core sample = 6.2cc)

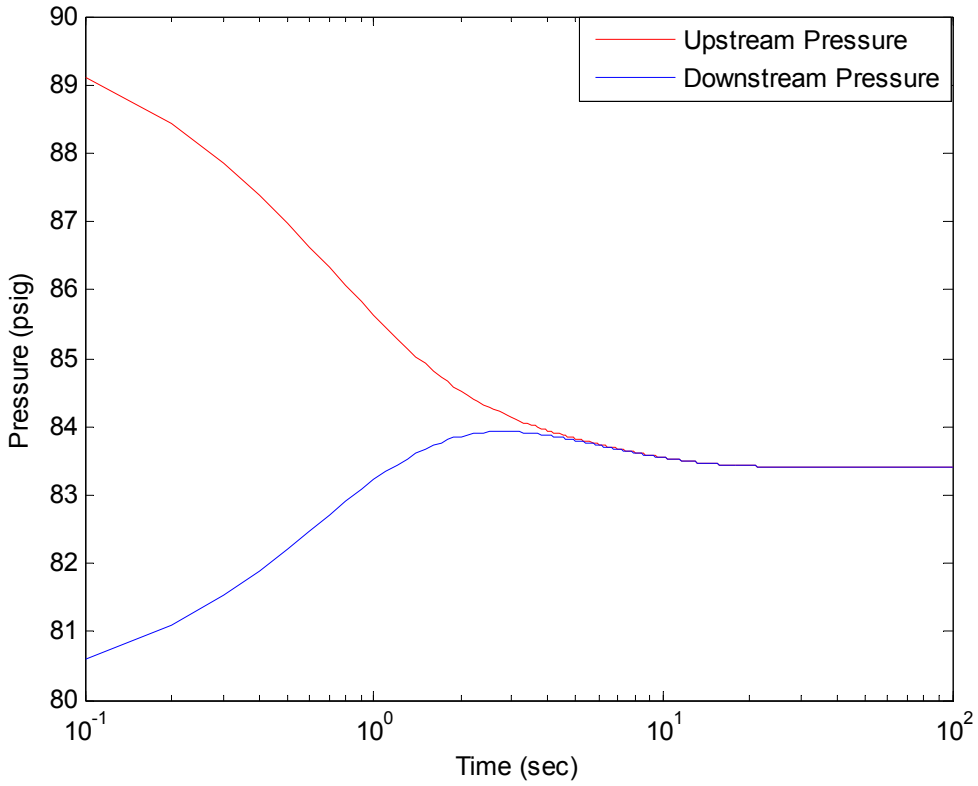

Figure 6-11 Effect of upstream and downstream reservoir volume on PPD curves for core BH8 ($V_u = V_d = 6cc$ & pore volume of the core sample = 6.2cc)

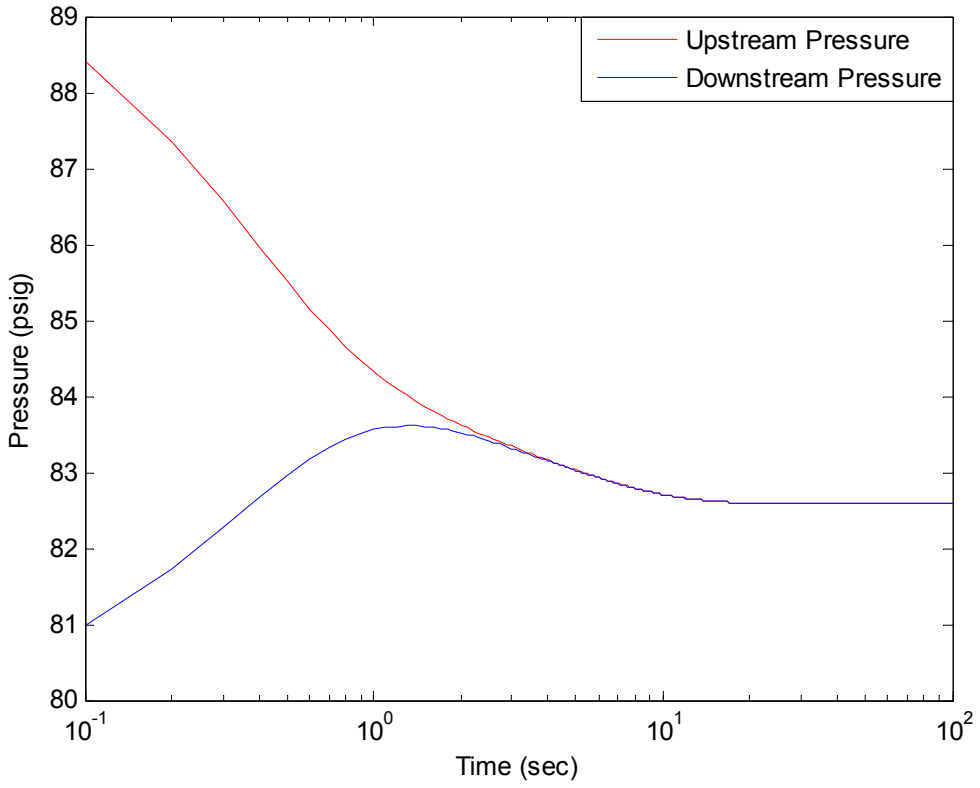

Figure 6-12 Effect of upstream and downstream reservoir volume on PPD curves for core BH8 ($V_u = V_d = 3cc$ & pore volume of the core sample = 6.2cc)

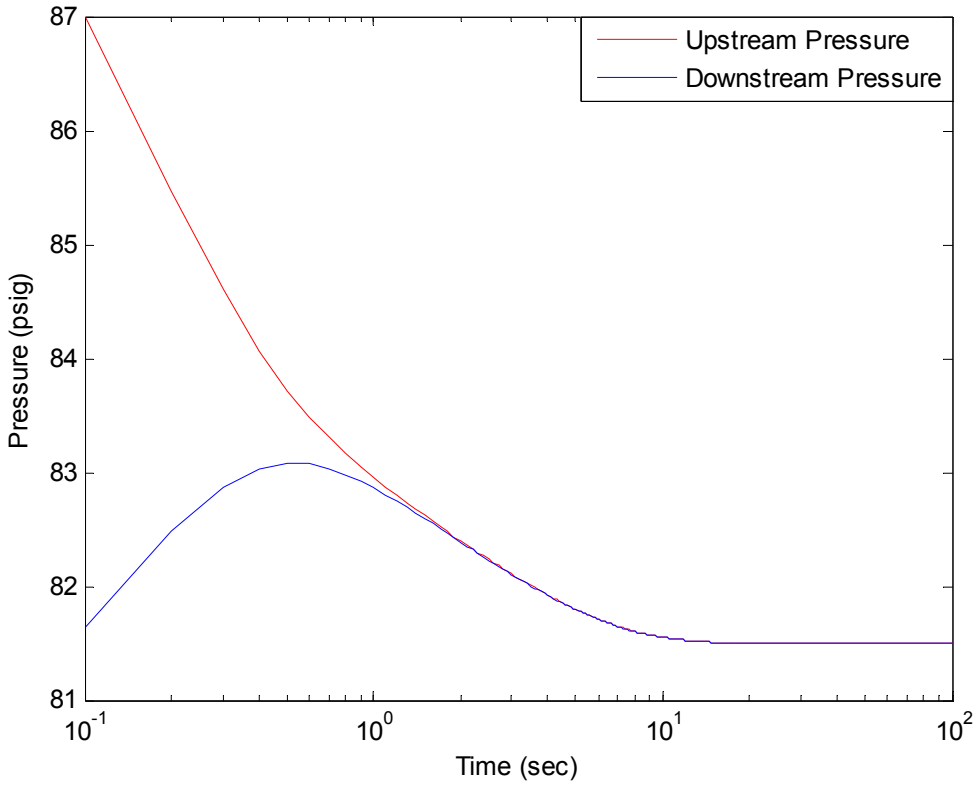

Figure 6-13 Effect of upstream and downstream reservoir volume on PPD curves for core BH8 ($V_u = V_d = 1.2cc$ & pore volume of the core sample = 6.2cc)

6.3 Effect of matrix permeability/fracture permeability ratio on pressure pulse decay curves

To study the effect of matrix permeability/fracture permeability ratio on pressure pulse decay curves, several simulation runs were performed. In this case, the value of matrix permeability is fixed at 0.1 *md* while the fracture permeability value is changed from 0.1 *md* to 1000 *md* and the values of other parameters such as porosity of matrix, porosity of fracture and the core samples dimensions which are used in the generation of simulation results are tabulated in Table 6.3 and the results of all runs are shown in Figure 6.14. The results indicate that when matrix permeability/fracture permeability ratio decreases less than 0.01, the effect of matrix permeability/fracture permeability ratio is clear on pressure pulse decay curves compare to the case of matrix permeability/fracture permeability ratio equals to 1. Therefore, the matrix permeability/fracture permeability ratio should be 0.01 or less to show the effect of fracture on the pressure pulse decay (PPD) curves.

Table 6-3 Fixed parameters used in the simulator input data

Core Sample ID	Core1
Length of the core sample (H)	5 cm
Radius of the core sample (R)	3.8 cm
Temperature (T)	$25^{\circ}c$
Porosity of matrix (ϕ_m)	10 %
Porosity of fracture (ϕ_f)	80%
Interporosity flow (λ)	10^{-6}
Area of matrix (A_m)	$0.99\,A$
Area of fracture (A_f)	$0.01\,A$

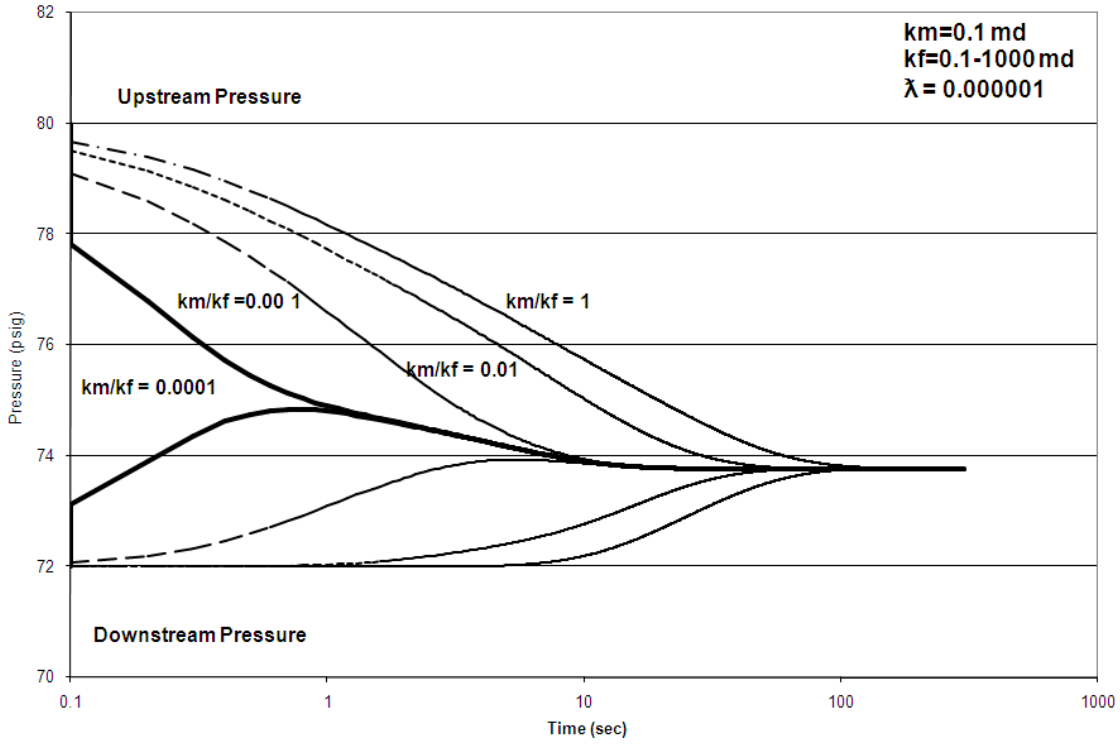

Figure 6-14 Effect of matrix permeability/fracture permeability ratio on pressure pulse decay curves.

6.4 Effect of gas slippage and interporosity flow parameter on pressure pulse decay curves

6.4.1 Effect of gas slippage on pressure pulse decay curves

Using the developed computer program, pressure pulse decay (PPD) data were generated in which gas slippage and interporosity flow parameter effects were incorporated. To show the effect of gas slippage on pressure pulse decay (PPD) curves, several simulation runs were performed for matrix permeability of 0.1 to 100 *md*. The values of other parameters such as porosity of matrix, porosity of fracture, temperature and the core samples dimensions which are used in the generation of simulation are tabulated in Table 6.3. The results of pressures drop are presented in Figures 6.15 to 6.18. These results indicate that the pressure pulse decay is faster in the gas slippage case as compared to the no gas slippage case. Therefore the permeability values appear to be higher as compared to actual value in the no gas slippage case. Furthermore, the gas slippage effect became less significant as the rock permeability increases.

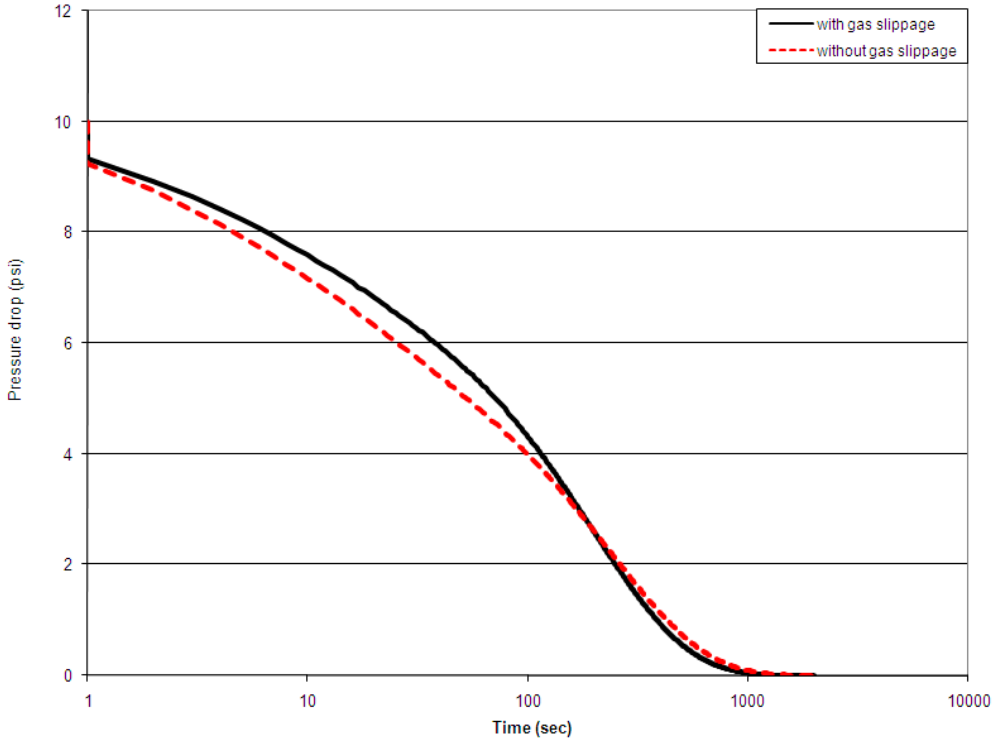

Figure 6-15 Effect of gas slippage on pressure pulse decay curves ($k_m = 0.01$).

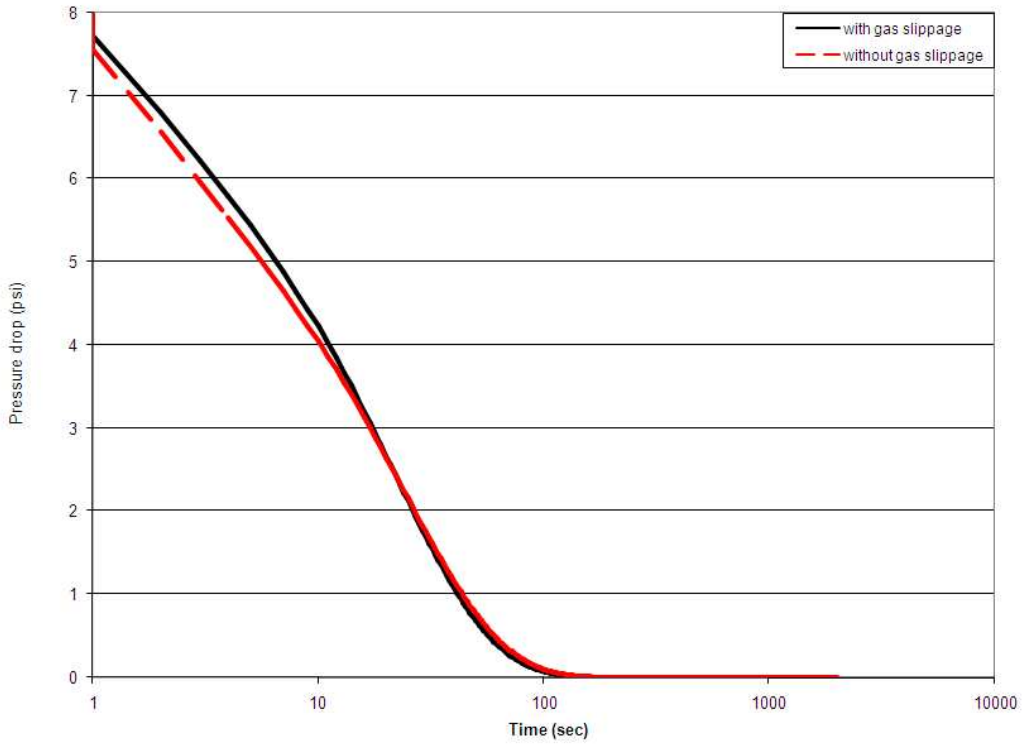

Figure 6-16 Effect of gas slippage on pressure pulse decay curves ($k_m = 0.1$).

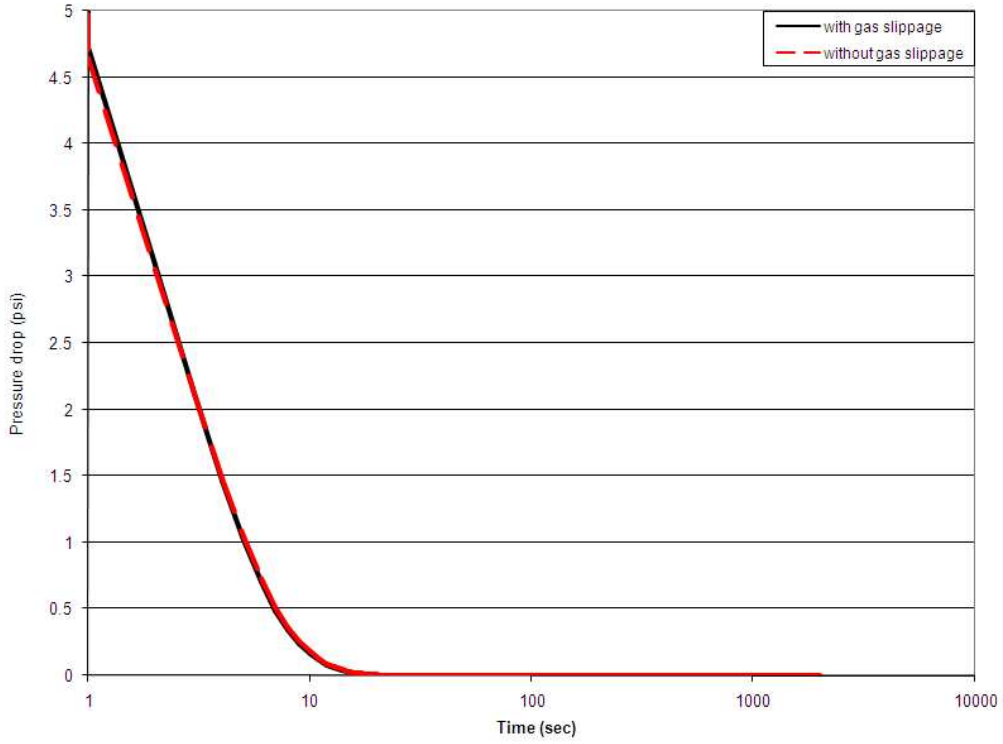

Figure 6-17 Effect of gas slippage on pressure pulse decay curves ($k_m = 1$).

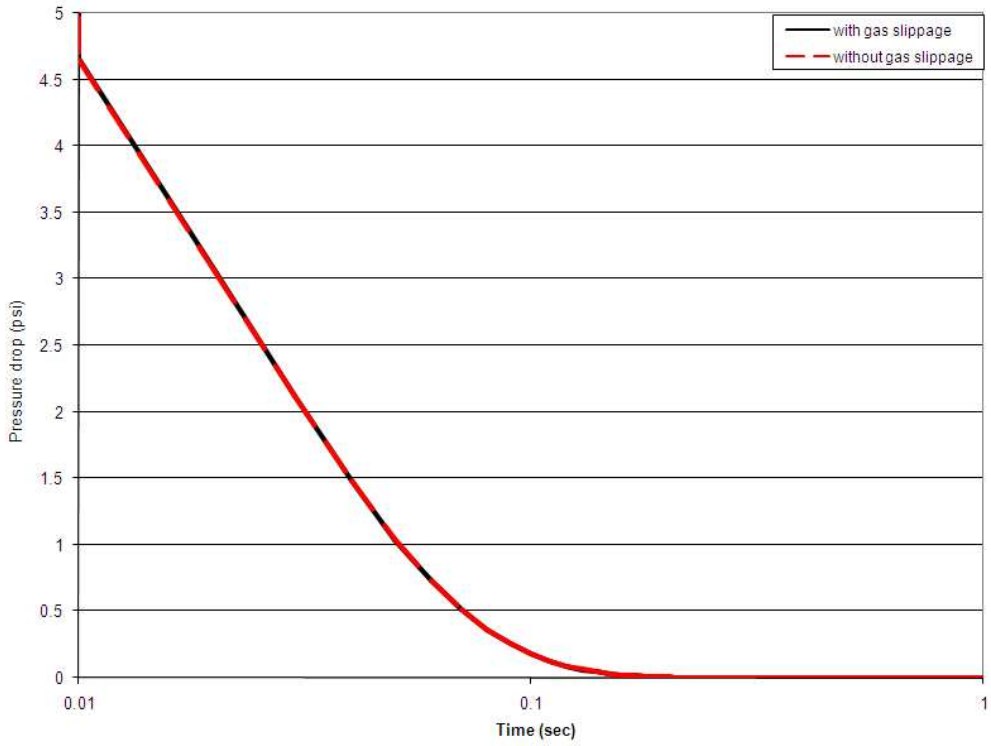

Figure 6-18 Effect of gas slippage on pressure pulse decay curves ($k_m = 100$).

6.4.2 Effect interporosity flow parameter on pressure pulse decay curves

To study the effect of interporosity flow parameter on pressure pulse decay (PPD) curves, several simulation runs were performed for interporosity flow parameters ranging from 0.01 to 1 and matrix and fracture permeabilities of 0.001 and 1000 *md*. The results are shown in Figure 6.19. These results indicate that when the value of interporosity flow parameter increases, gas flow from fracture through the matrix increases due to the larger exchange between matrix and fracture. Therefore the effect of fracture on pressure pulse decay curve increases. On the other hand, when interporosity flow parameter is equal to zero, there is no flow of gas from fracture to the matrix but the gas flows from upstream cell and downstream cell through the matrix and this causes the pressure pulse decay curve to decrease at large time.

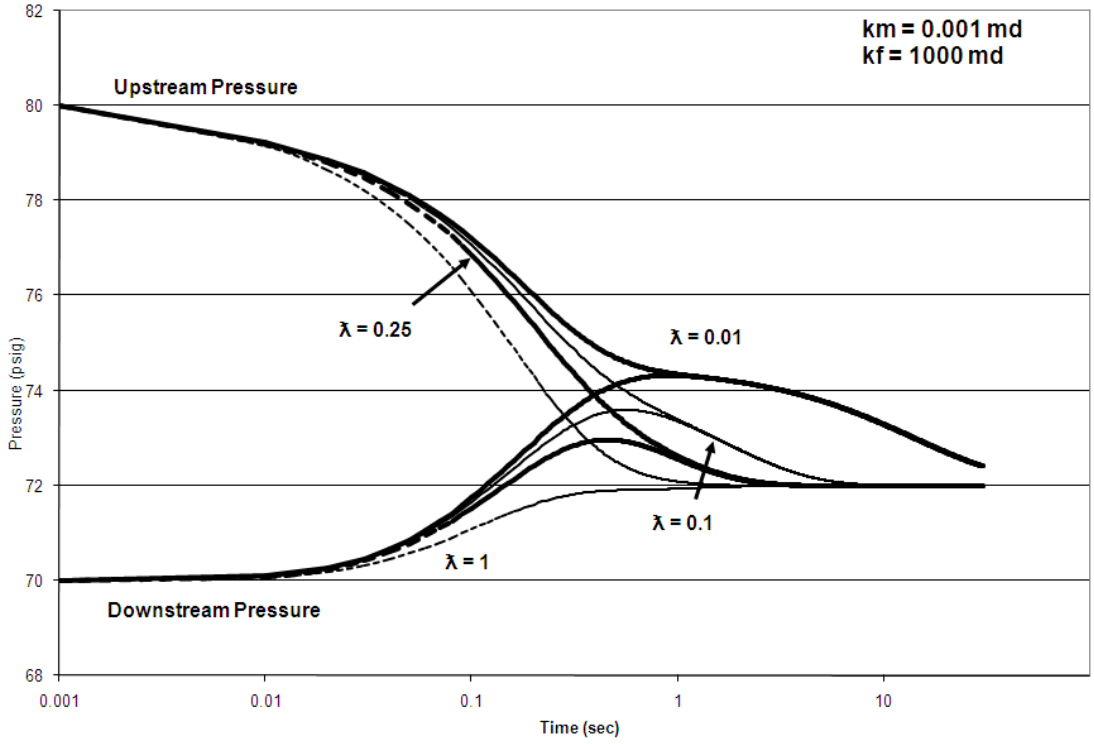

Figure 6-19 Effect of interporosity flow parameter on pressure pulse decay curves

6.5 Effect of the area of fracture on pressure pulse decay curves

It is difficult to estimate the area of the fracture, for this reason first the area of all system (core sample) is calculated by assuming there is only matrix and then the fracture area is assumed as a percent of the area of all system. In this part, the effect of the area of the fracture on pressure pulse decay curves is studied. Several runs were performed for the area of fracture ranging from 0.01 % to 0.0001% of the area of the core sample for matrix permeability of 0.001 *md* and fracture permeability of 1000 *md*. The values of other parameters such as porosity of matrix, porosity of fracture, temperature and the core sample dimensions used in the generation of simulation results are tabulated in Table 6.3. The results are shown in Figure 6.20. These results indicate that the fracture area affects both upstream and downstream pressure pulse decay curves as shown in Figure 6.20.

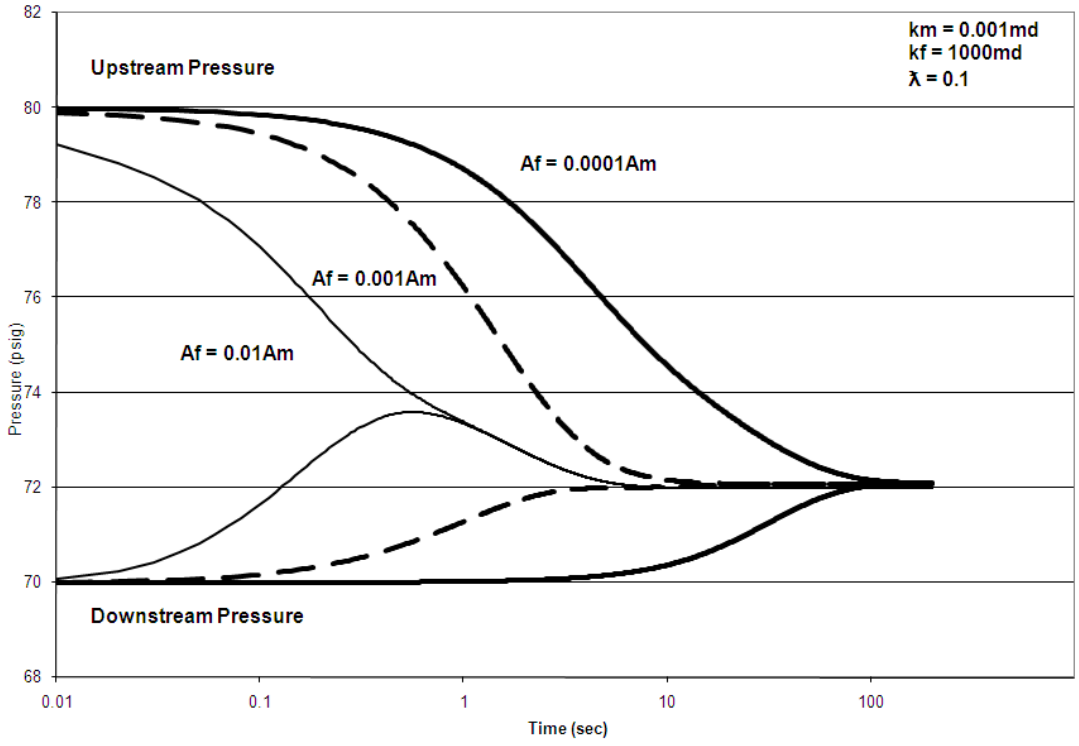

Figure 6-20 Effect of the area of fracture on pressure pulse decay curve

6.6 Validation of the developed computer program

In this part, the evaluation of the non-linear regression computer program to analyze the pressure pulse decay data is presented. Experimental pressure pulse decay data were generated using the OPP pressure pulse decay equipment for permeability values ranging from about 0.1 to 2 *md*. The permeabilities of the tested core samples were obtained using Jones[15] technique.

6.6.1 Estimation of permeability using developed computer program

The experimental pressure pulse decay data were analyzed by using the developed computer program. The results are listed in Table 6.4. Figures 6.21 to 6.23 show the upstream pressure vs. time curves of the selected core samples for the pressure pulse decay data. Analysis of the data using the non-linear regression computer program gives the estimate permeability. The obtained results indicate close agreement between the estimated permeabilities by the program and Jones method.

Table 6-4 Analysis of simulation pulse decay data using developed computer program

Core #	ΔP_i (psi)	Jones method	Program output
		k (md)	k (md)
Core A	190	11.57	8.8377
Core B	192	1.0746	0.94571
Core C	160	148.1	125.25

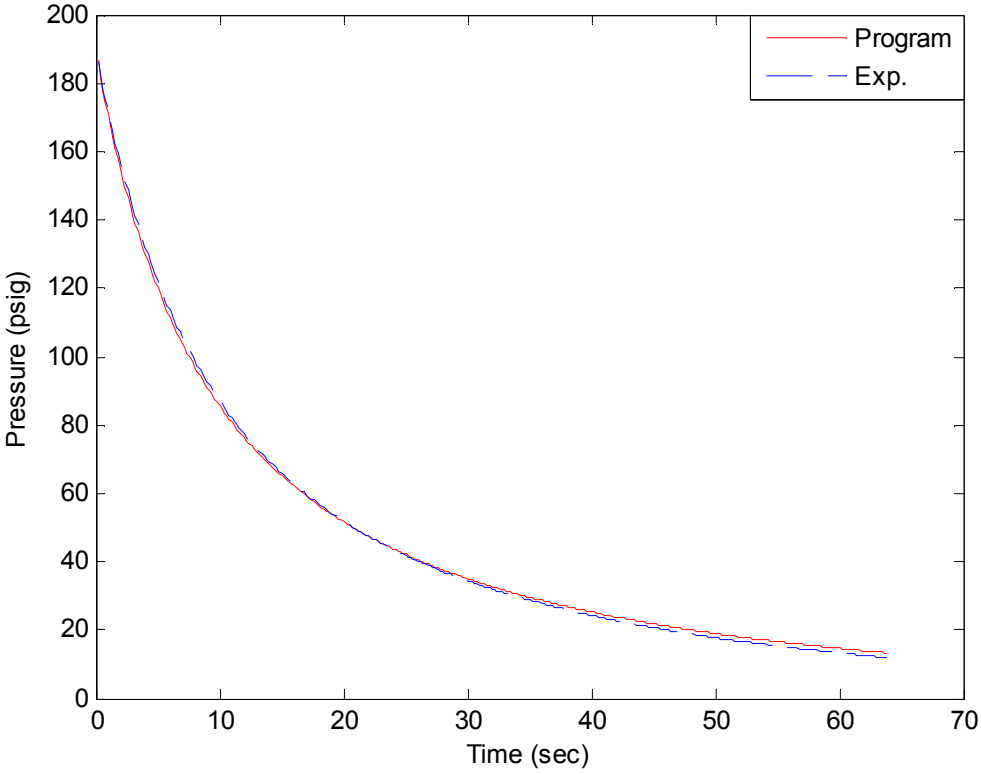

Figure 6-21 Pressure difference vs. time curve fitting for core A

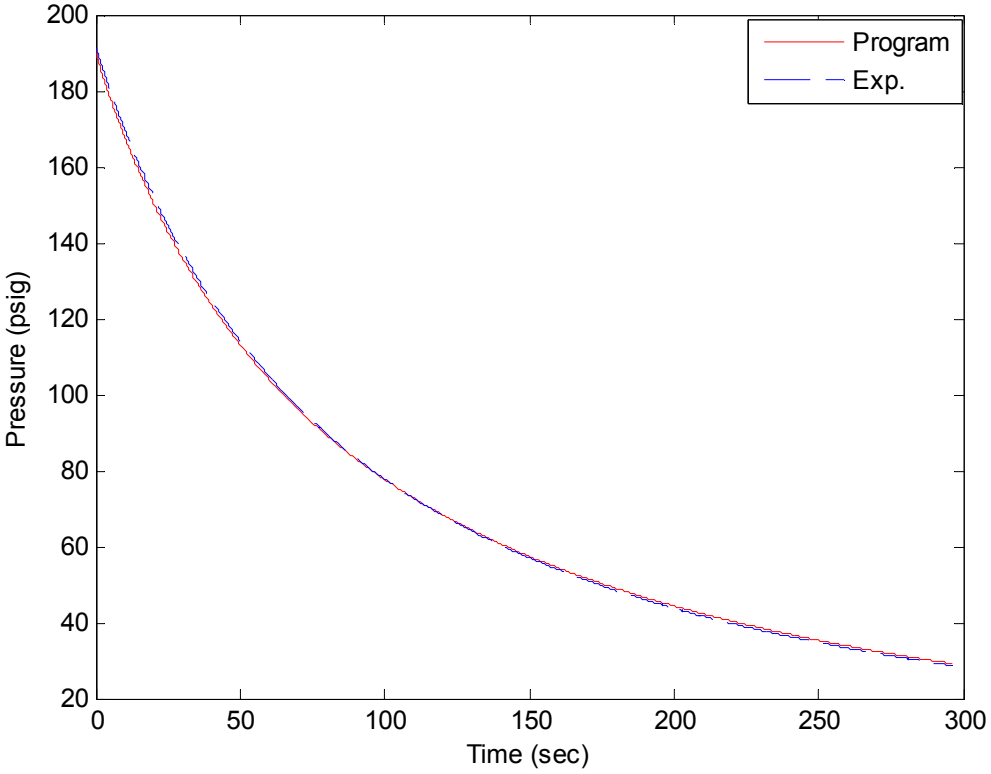

Figure 6-22 Pressure difference vs. time curve fitting for core B

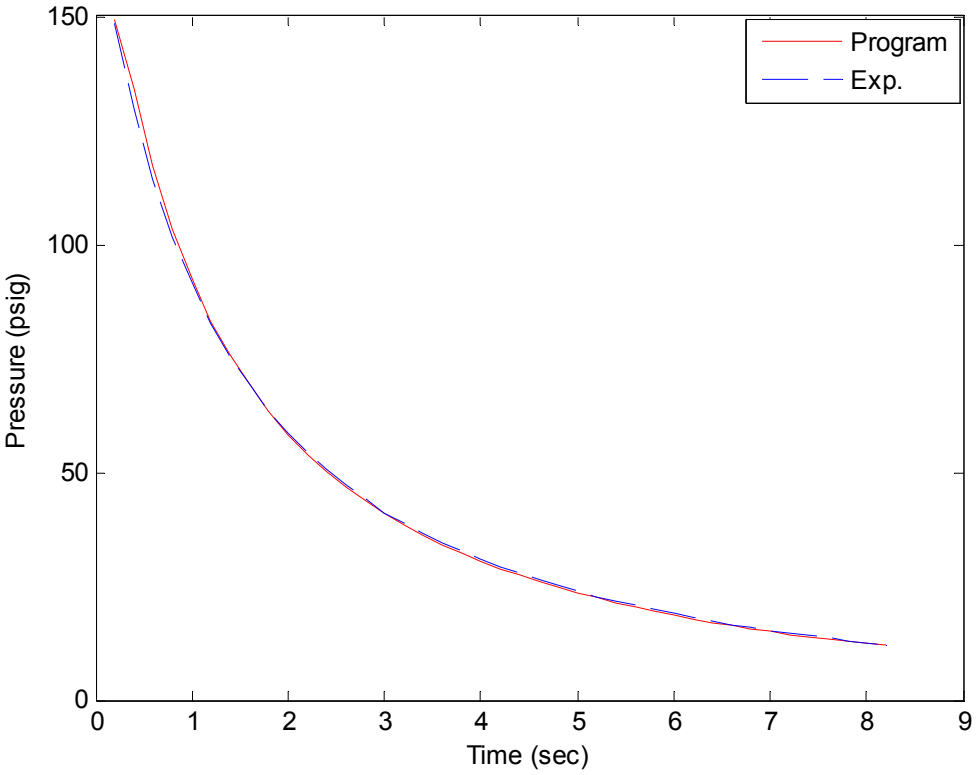

Figure 6-23 Pressure difference vs. time curve fitting for core C

6.7 Analysis of experimental pressure pulse decay data using developed computer program

The estimation of matrix and fracture permeabilities was the main objective of this study. Two core samples were selected to perform pressure pulse decay tests. Using the setup presented before (chapter 5), several pressure pulse decay experiments were performed under different experimental conditions with low value of pressure pulse. The reasons for not using large pressure pulse were,

- Non-Darcy flow effects.
- Gas expansion from high pressure that could cause cooling effects.

Table 6.5 shows the properties of the core samples and the experimental conditions for all the pressure pulse decay experiments.

Table 6-5 Core samples and experimental conditions input data

Core properties				
Core #	Length (cm)	Diameter (cm)	Porosity %	
CS 1	11.92	10.05	13.56	
CS 2	11.58	10.58	12.7	
Experimental conditions				
Upstream reservoir volume (cc)	Downstream reservoir volume (cc)	Temperature $\left({}^{o}c\right)$	Number of grid cell in X-Direction	Number of grid cell in Y-Direction
8.34	7.37	25	10	5

6.7.1 Determination of matrix and fracture permeabilities

For each of the two core samples, pressure pulse decay experiment tests were conducted at pressure difference of about 5 psi. Then the obtained pressure pulse decay data for both core samples were analyzed by using the developed computer program to estimate the matrix and fracture permeabilities. As discussed in section 6.2, both of the upstream and downstream reservoirs were selected to have close volumes and also volumes of both upstream and downstream reservoirs were less than 20% of pore volume of the core sample.

Because the core samples used do not have natural fractures, a fracture was created by cutting the core samples into two halves. Before cutting the core sample, the matrix porosity of the core sample was measured. Then after cutting the core sample, the matrix-fracture porosity was measure. After that the fracture porosity was calculated from this measurement value. The obtained fracture porosity of core sample CS 1 is 85.2 % and 81.36 % for core sample CS 2 .Finally the fractured core samples were tested. The data were analyzed to obtain the matrix and fracture permeabilities and interporosity flow parameter. The results are listed in Table 6.6. Figures 6.24 to 6.27 show upstream cell pressure and downstream cell pressure vs. time curve fitting of the selected core samples for the pressure pulse decay data.

Table 6-6 Analysis of the experimental pressure pulse decay data using developed computer program (matrix-fracture system)

Core #	Pressure size	Program out							
	ΔP (psi)	Permeability (md)				Interporosity flow		Gas slippage	
		Horizontal (matrix)	Vertical (matrix)	Horizontal (fracture)	Vertical (fracture)	Horizontal (fracture)	Vertical (fracture)	Horizontal (matrix)	Vertical (matrix)
CS 1	7	0.0186	0.047	59511	245000	0.00038	0.0814	28.962	20.773
CS 2	6	0.010	0.0104	9355	20558	0.00017	0.0062	36.212	35.739

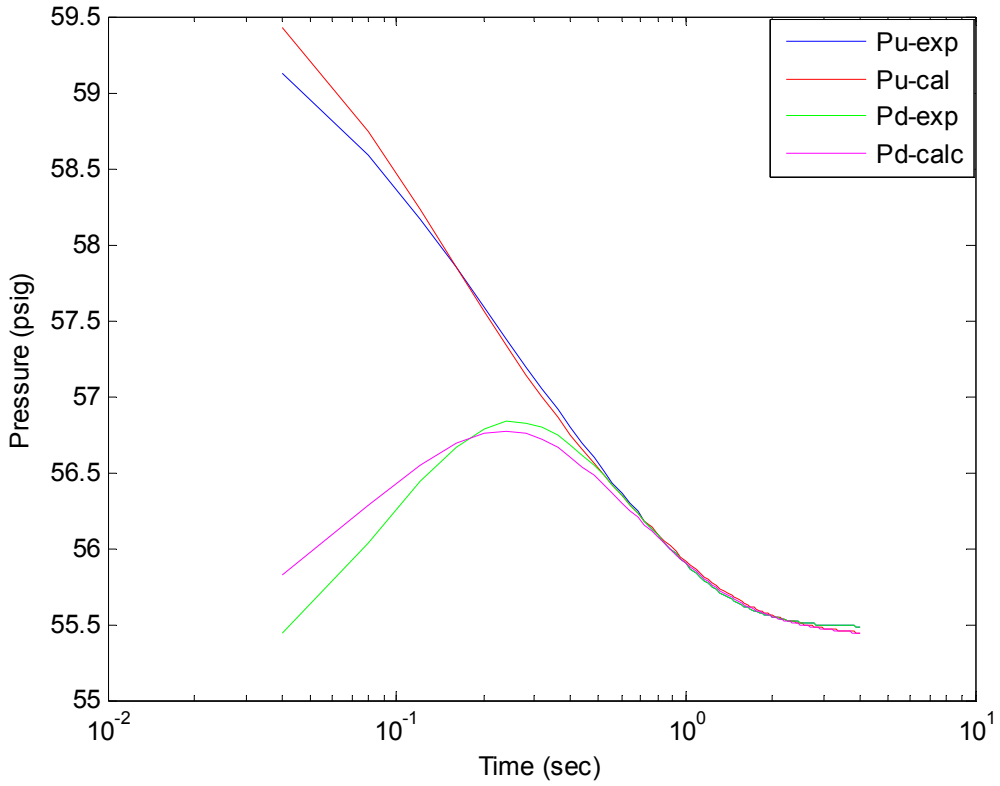

Figure 6-24 Experimental data analysis using the developed computer program for CS 1 (Fracture permeability vertical)

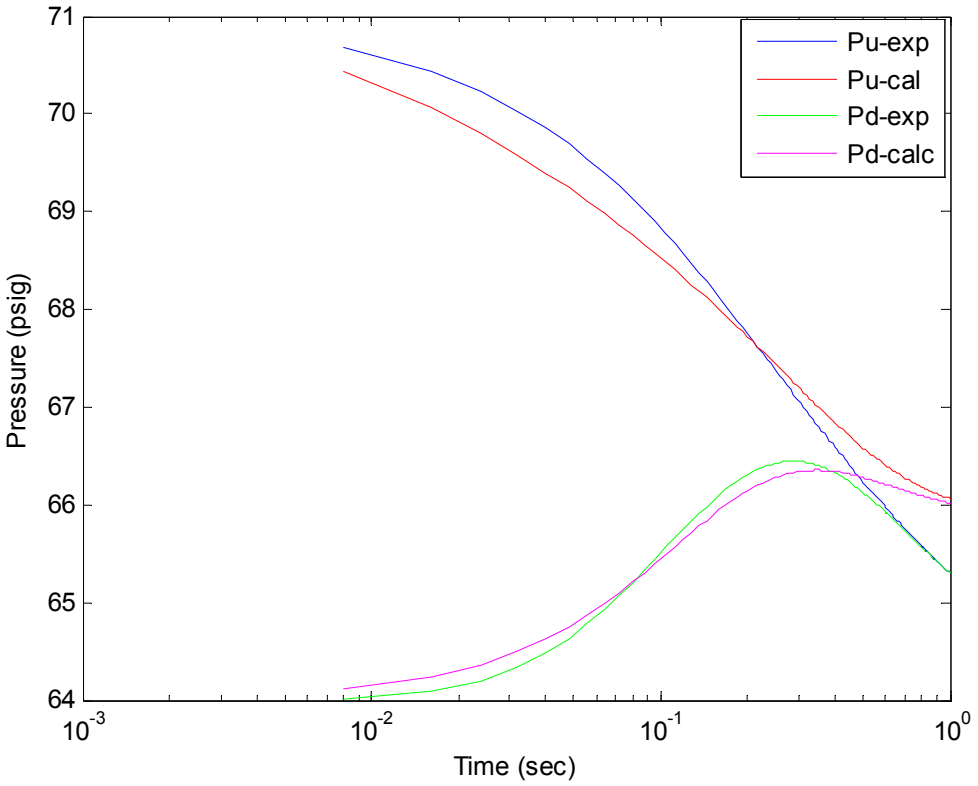

Figure 6-25 Experimental data analysis using the developed computer program for CS 1 (Fracture permeability Horizontal)

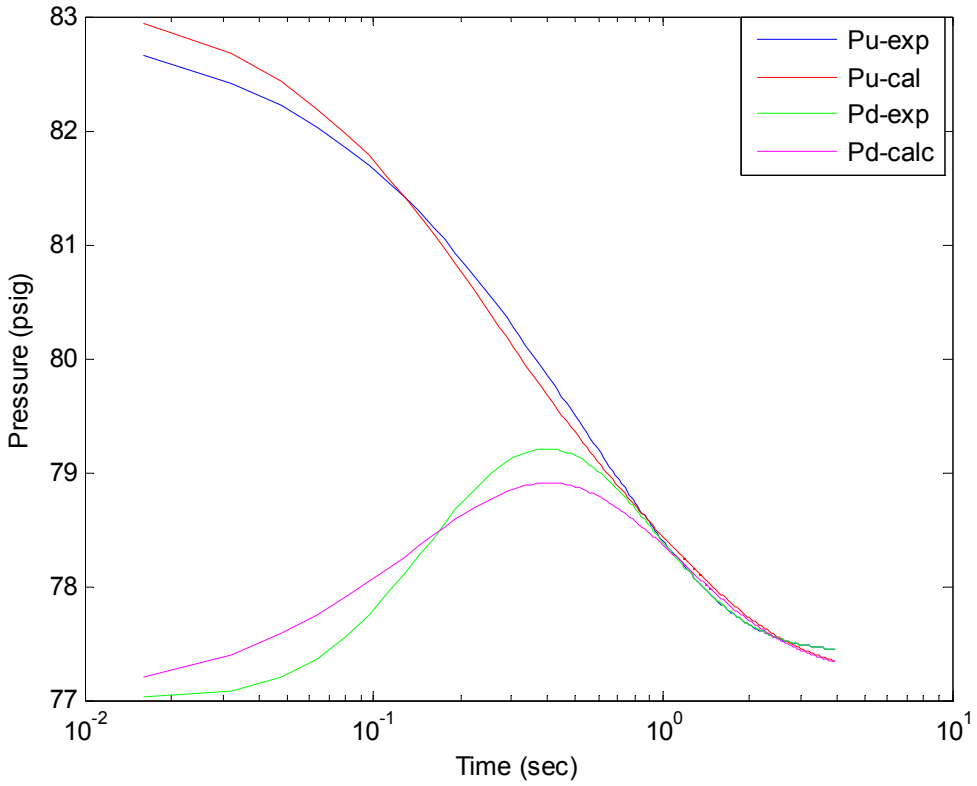

Figure 6-26 Experimental data analysis using the developed computer program for CS 2 (Fracture permeability Vertical)

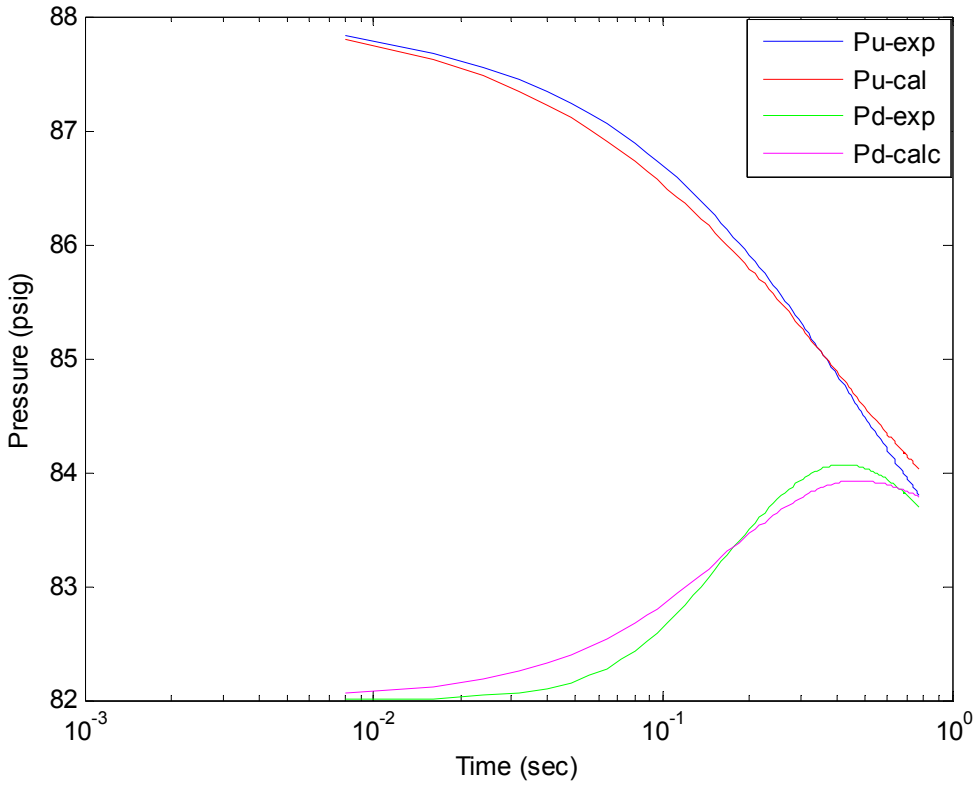

Figure 6-27 Experimental data analysis using the developed computer program for CS 2 (Fracture permeability Horizontal)

CHAPTER 7

CONCLUSIONS

The aim of this study was to investigate the application of pressure pulse decay method for determining the matrix and fracture permeabilities of fractured whole core samples. Based on the results of this study, the following conclusion can be deduced:

1. A mathematical model has been developed to solve the transient, compressible fluid flow equation to describe pressure pulse decay method in fractured whole core samples.

2. A computer program has been developed that analyzes the pressure pulse decay data to estimate the matrix and fracture permeabilities using non-linear regression.

3. Upstream and downstream reservoir volumes affect the pressure pulse decay responses if upstream and downstream reservoir volumes are equal to 20% or less of the pore volume of the core sample.

4. The effect of matrix permeability/fracture permeability ratio on pressure pulse decay response is clear if matrix permeability/fracture permeability ratio is less than 0.05.

5. The larger the interporosity flow parameter the more distinguished the pressure pulse decay response compare to the case of no inter-flow between matrix and fracture.

6. The pressure pulse decay technique can be used for the estimation of matrix and fracture permeabilities of whole core samples.

REFERENCES

1. Alan, M. Sibbit: "Quantifying Porosity and Estimating Permeability from Well Logs in Fractured Basement Reservoir," SPE paper 130157, SPE Petro Vietnam held in Vietnam, March 1995.

2. Amaefule, J.O. et al.: "Laboratory Determination of Effective Liquid Permeability in Low-Quality Reservoir Rocks by the Pulse Decay Technique," paper SPE 15149 presented at the 1986 SPE California Regional Meeting, Oakland, 2 – 4 April.

3. American Petroleum Institute, "Recommended Practiced for Core Analysis," RP-40, Second Edition, February 1998.

4. Asfari, A. and Witherspoon, P. A.: "Numerical Simulation of Naturally Fractured Reservoir," SPE paper 429, Soc. Pet. Eng. Of AIME held in Houston, Tex., 10 – 12 January, 1973.

5. Bourbie, T. and Walls, J.: "Pulse Decay Permeability: Analytical Solution and Experimental Test," Society of Petroleum Engineers Journal, October 1982, PP. 719 - 721.

6. Brace, W. F., Walsh, J. B. and Frangos, W. T.:"Permeability of Granite under High Pressure," Journal of Geophysical Research, Vol. 73, NO. 6, March 15, 1968.

7. Chen, T. and Stagg, P. W.: "Semi-Log Analysis of the Pulse-Decay Technique of permeability Measurement," Society Petroleum Engineers Journal, December 1984, PP 632-642.

8. Collins, R.E.: "Flow of Fluids through Porous Materials," The Petroleum Publishing Company, 1976, PP. 88-98.

9. Dicker, Al. and Smits, R.M.: "A Practical Approach for Determining Permeability from Laboratory Pressure-Pulse Decay Measurements, "SPE paper 17578 presented at the 1988 SPE International Meeting on Petroleum Engineering, Tianjin, China, 1 - 4 November.

10. Gilicz, A.: "Application of the Pulse Decay Technique," SPE paper 22688 presented at the 66th Annual Technical Conference and Exhibition of the SPE held in Dallas, TX, October 6-9, 1991.

11. Guo, F. and Wong, K.: "A New Pressure Technique Measurement of Live Heavy Oil Mobility in Unconsolidated Oil Sand Cores, "The journal of Canadian Petroleum Technology, Vol. 35, No. 1, January 1996, P.P 60 – 66.

12. Hamid, Jalal.: "Application of Pulse Decay Technique to Characterize Whole Cores," MS. Thesis, KFUPM, 2000.

13. Hirasaki, G.T. and O'Dell, P.M.: "Representation of Reservoir Geometry for Numerical Simulation," Society Petroleum Engineers Journal, December 1970, PP 393 - 404.

14. Haskett, Stevem E., Narahara, Gene M. and Holditch, Stephen A.: "A Method of Simultaneous Determination of Permeability and Porosity in Low-Permeability Cores," SPE Formation Evaluation, September 1988, PP. 651 – 658

15. Jones, S.C: "A Technique for Faster Pulse-Decay Permeability Measurements in Tight Rocks,"SPE paper 28450 presented at the 69th Annual Technical

Conference and Exhibition of the SPE held in New Orleans, LA, September 25 - 28, 1994, PP. 907 - 914.

16. Jones, S.C: "A Rapid Accurate Unsteady State Klinkenberg Permeameter," SPEJ, October 1972.

17. Kamath, J., Boyer, R. E. and Nakagawa, F.M.: "Characterization of Core-Scale Heterogeneities Using Laboratory Pressure Transients," SPE Formation Evaluation, September 1992, PP. 219 - 227.

18. Kazemi, H.: "Pressure Transient Analysis of Naturally Fractured Reservoirs," Society Petroleum Engineers Journal, December 1969, Vol. 246, PP 632-642.

19. Neilson Rudd: "Pressure Decay Measurement," SPE 1604, presented at the SPE Gas Technique Symposium, Omaha, Nebr. September 15-16, 1966.

20. Ning Xiuxu. Et al: "The Measurement of Matrix and Fracture Properties in Naturally Fractured Cores,"SPE paper 25898 presented at the SPE Rocky Mountain Regional/Low Permeability Reservoirs Symposium held in Denver, CO, U.S.A., April 12 -14, 1993.

21. Noman, Muhammad: "Incorporating the Effects of Gas Slippage and Non-Darcy Flow in the Measurement of Permeability Using Pressure Pulse Decay Technique," MS. Thesis, KFUPM, 2000.

22. Odeh, A.S. and Mcmillen, J. M.: "Pulse Testing: Mathematical Analysis and Experimental Verification oil,"SPE paper 3536 presented at SPE 46th Annual Fall Meeting held in New Orleans, October 3 - 6, 1971.

23. Odeh, A.S.: "Unsteady-State behaviour of Naturally Fractured reservoirs," Society Petroleum Engineers Journal, March 1965, Vol. 234, PP 60 - 66.

24. Pollard, P.: "Evaluation of Acid Treatments from Pressure Build-up Analysis," Trans., AIME, February 1959, Vol. 216, PP 38-43.

25. Prats, M.: "The Influence of Oriented Arrays of Thin Impermeable Shale Lenses or Highly Conductive Natural Fracture Apparent Permeability Anisotropy," J. Pet. Tech., October 1972, PP 1219-1221.

26. Richard, O. Baker and Frank Kupper: "Reservoir Characterization for Naturally Fractured Reservoir,"SPE paper 63286, Annual Technical Conference and Exhibition held in Dallas, Texas 1-4 October 2000.

27. Sabathier, J. C., Bourbiaux, B. J. and Sarda, A.: "A New Approach of Fractured Reservoirs,"SPE paper 39825, presented at SPE International Petroleum Conference and Exhibition of Mexico held in Villahermosa, Mexico, 3 – 5 March 1998.

28. Sandro Arange, Eduardo A. Idrobo and Hector H. Perez: "A New Methodology to Estimate Fracture Intensity Index for Naturally Fractured Reservoir," Paper SPE 86935, presented at SPE International Thermal Operations and Heavy Oil Symposium and Western Regional Meeting held in Bakersfield, California, U.S.A., 16-18 March 2004.

29. Sonier, F. and Chaumet, P.: "A Fully Implicit Three-Dimensional Model in Curvilinear Coordinates," Society Petroleum Engineers Journal, August 1974, PP 361 - 370.

30. Warren, J. E. and Root, P. J.: "The Behaviour of Naturally fractured Reservoirs," Society Petroleum Engineers Journal, September 1963, Vol. 228, PP 245 - 255.

31. Yamada, S. E. and Jones, A. H..: "A Review of a Pulse Technique for Permeability Measurements," SPEJ Forum, October 1980, PP. 357 - 358

VITA

Name Khaled Saeed Ahmed Bajaalah

E-mail Address kh_bajalah@hotmail.com

Education

University Obtained B.E in Petroleum Engineering from Hadhramout University of Science and Technology, Yemen, 2002

Obtained M.S in Petroleum Engineering from King Fahd University of Petroleum & Minerals, Dhahran, KSA, 2009.

Work Experience

2002 to 2004 Assigned as instructor in Hadhramout University of Science and Technology in Yemen.

I still worked in Hadhramout University of Science and Technology.

Major Achievements and Awards

Received First Honor Awards in all the semesters in the BS program.